Original Article

MOLECULAR METABOLISM

Treatment of infantile-onset Pompe disease in a rat model with muscle-directed AAV gene therapy

Sergio Muñoz[1,2,3,10], Joan Bertolin[1,2,10], Veronica Jimenez[1,2,3,10], Maria Luisa Jaén[1,2,3], Miquel Garcia[1,2,3], Anna Pujol[1,2], Laia Vilà[1,2,3], Victor Sacristan[1,2,3], Elena Barbon[5], Giuseppe Ronzitti[5], Jihad El Andari[4], Warut Tulalamba[7,8], Quang Hong Pham[7,8], Jesus Ruberte[1,6], Thierry VandenDriessche[7,8], Marinee K. Chuah[7,8], Dirk Grimm[4,9], Federico Mingozzi[5], Fatima Bosch[1,2,3,*]

ABSTRACT

Objective: Pompe disease (PD) is caused by deficiency of the lysosomal enzyme acid α-glucosidase (GAA), leading to progressive glycogen accumulation and severe myopathy with progressive muscle weakness. In the Infantile-Onset PD (IOPD), death generally occurs <1 year of age. There is no cure for IOPD. Mouse models of PD do not completely reproduce human IOPD severity. Our main objective was to generate the first IOPD rat model to assess an innovative muscle-directed adeno-associated viral (AAV) vector-mediated gene therapy.

Methods: PD rats were generated by CRISPR/Cas9 technology. The novel highly myotropic bioengineered capsid AAVMYO3 and an optimized muscle-specific promoter in conjunction with a transcriptional cis-regulatory element were used to achieve robust *Gaa* expression in the entire muscular system. Several metabolic, molecular, histopathological, and functional parameters were measured.

Results: PD rats showed early-onset widespread glycogen accumulation, hepato- and cardiomegaly, decreased body and tissue weight, severe impaired muscle function and decreased survival, closely resembling human IOPD. Treatment with AAVMYO3-Gaa vectors resulted in widespread expression of *Gaa* in muscle throughout the body, normalizing glycogen storage pathology, restoring muscle mass and strength, counteracting cardiomegaly and normalizing survival rate.

Conclusions: This gene therapy holds great potential to treat glycogen metabolism alterations in IOPD. Moreover, the AAV-mediated approach may be exploited for other inherited muscle diseases, which also are limited by the inefficient widespread delivery of therapeutic transgenes throughout the muscular system.

Keywords Glycogen metabolism; Myopathies; Pompe disease; Rat model; Gene therapy; AAV

1. INTRODUCTION

Pompe disease (PD) (Glycogen storage disease type II, OMIM #232300) is a rare metabolic autosomal recessive lysosomal storage disease caused by mutations in the gene coding for acid alpha-glucosidase (GAA, EC 3.2.1.20) [1]. The absence of this lysosomal enzyme leads to accumulation of undegraded glycogen, mainly in skeletal and cardiac muscle, causing progressive severe myopathy [1]. Recent studies have also reported glycogen accumulation in the central and peripheral nervous system of PD patients [2–4]. The clinical presentation of PD is a spectrum of phenotypes varying in age of onset, organ involvement, severity of disease, and rate of progression according to residual GAA enzymatic activity [1,5]. Infantile-onset Pompe disease (IOPD) is caused by a severe or complete GAA deficiency with <1% residual enzyme activity [5]. Clinical features are related to neonatal onset and rapidly progressive muscular pathology, leading to skeletal muscle weakness and hypotonia, cardiomegaly and respiratory failure, due to the malfunctioning of diaphragm and respiratory muscles [1]. Late-onset Pompe disease (LOPD) is caused by only a partial deficiency (<30% residual activity) of GAA [5]. Patients with LOPD have a more

[1]Center of Animal Biotechnology and Gene Therapy (CBATEG), Universitat Autònoma de Barcelona, 08193, Bellaterra, Spain [2]Department of Biochemistry and Molecular Biology, Universitat Autònoma de Barcelona, 08193, Bellaterra, Spain [3]Centro de Investigación Biomédica en Red de Diabetes y Enfermedades Metabólicas Asociadas, Instituto de Salud Carlos III, Spain [4]Department of Infectious Diseases/Virology, Section Viral Vector Technologies, BioQuant Center, Medical Faculty, University of Heidelberg, 69120, Heidelberg, Germany [5]INTEGRARE, Genethon, INSERM UMR951, Univ Evry, Université Paris-Saclay, 91002, Evry, France [6]Department of Animal Health and Anatomy, School of Veterinary Medicine, Universitat Autònoma de Barcelona, 08193, Bellaterra, Spain [7]Department of Gene Therapy & Regenerative Medicine, Vrije Universiteit Brussel (VUB), B-1090, Brussels, Belgium [8]Department of Cardiovascular Sciences, Center for Molecular & Vascular Biology, University of Leuven, 3000, Leuven, Belgium [9]German Center for Infection Research (DZIF) and German Center for Cardiovascular Research (DZHK), Partner site Heidelberg, Heidelberg, Germany

[10] Sergio Muñoz, Joan Bertolin and Veronica Jimenez contributed equally to this work.

*Corresponding author. Center of Animal Biotechnology and Gene Therapy (CBATEG), Universitat Autònoma de Barcelona, 08193, Bellaterra, Spain. E-mail: fatima.bosch@uab.es (F. Bosch).

Received July 31, 2023 • Revision received January 3, 2024 • Accepted February 7, 2024 • Available online 10 February 2024

https://doi.org/10.1016/j.molmet.2024.101899

Abbreviations

PD	Pompe Disease
IOPD	infantile-onset Pompe Disease
LOPD	late-onset Pompe Disease
Gaa	lysosomal enzyme acid α-glucosidase
CRE	cis-regulatory element
ERT	enzyme replacement therapy
rhGAA	recombinant human GAA
AAV	adeno-associated viral vector
KI	knock-in
KO	knock-out
sgRNA	single guide RNA
WT	wild-type animals
PAS	Periodic acid Schiff
TEM	transmission electron microscopy
CNS	central nervous system
SC	spinal cord
XLMTM	X-linked myotubular myopathy
DRG	dorsal root ganglion
DMD	Duchenne Muscular Dystrophy

slowly progressive skeletal myopathy eventually resulting in mobility problems and respiratory difficulties, but generally do not present with hypertrophic cardiomyopathy [1]. In IOPD, death generally occurs during the first year of life due to a cardiorespiratory failure, although the less severe forms have longer life expectancy [1].

To date, the only treatment approved for PD is an enzyme replacement therapy (ERT) based on intravenous administrations of recombinant human GAA (rhGAA) [5]. However, this therapy needs repeated infusions of high doses of rhGAA and presents reduced efficacy, mainly due to limited enzyme uptake in key affected tissues and the possibility of severe immune responses that neutralize the therapeutic rhGAA protein [6]. To overcome the limitations of ERT, a variety of *in vivo* adeno-associated viral (AAV) vector-mediated gene therapy approaches have been developed for PD [6–8]. Nevertheless, to achieve therapeutic benefit in skeletal and cardiac muscle is challenging. The GAA enzyme is not efficiently secreted and it is difficult to achieve AAV-mediated widespread *Gaa* gene transfer to affected muscles [9–12]. To overcome these drawbacks, liver-directed AAV-based approaches using engineered secretable GAA that will be taken up by affected tissues have been developed [13–17]. Other strategies use AAV capsids displaying efficient muscle tropism, together with muscle-specific promoters, delivered systemically or intramuscularly to increase *Gaa* expression in muscle, although liver transduction has also been reported [9,18–23]. Several of these approaches have already reached clinical application, and phase I/II clinical trials are presently ongoing (ClinicalTrials.gov Identifiers: NCT00976352, NCT02240407, NCT03533673, NCT04093349, NCT04174105).

While liver-directed gene therapy may be suitable for adult patients, due to the predominantly non-integrative nature of AAV vectors, this strategy might not be the best option for IOPD because of hepatocyte replication occurring in young children [24–26]. Consequently, this hepatocyte replication would inevitably result in a dilution of the non-integrated AAV episomes harboring the therapeutic GAA transgene and a subsequent decline in GAA expression. These limitations of liver-directed gene transfer could potentially be overcome by directly targeting the affected skeletal muscles and heart in IOPD, which are most non-dividing. However, systemic AAV delivery to target muscle can be challenging, as it requires high vector doses, which can be associated with off target transduction and organ toxicities, notably in the liver [23,27]. To this end, development of highly muscle-specific AAV capsids is under extensive investigation [28–30]. We have recently described a novel myotropic AAVMYO3 capsid by combining a myotropic shuffled AAV capsid with a muscle-specific P1 peptide that outperformed the gold standard AAV8 and AAV9 vectors in mice, while dramatically reducing liver transduction [31].

Here, we have engineered AAVMYO3 vectors expressing GAA under the control of muscle-targeted promoter/transcriptional *cis*-regulatory element (CRE) [32] to treat IOPD. To overcome the limitations of the existing mouse models of PD, which do not fully develop the critical features of human IOPD [13–16,20,21,33–40], a new PD rat model was developed. This newly generated PD rat model that suffered from devastating alterations characteristic of IOPD patients was used to test the efficacy of the gene therapy. Treatment of PD rats with AAVMYO3-*Gaa* vectors resulted in highly efficient transduction of skeletal and cardiac muscles that fully reversed muscle metabolic, morphological, and functional alterations and normalized animal survival. These results represent an important step towards the future clinical translation of this approach for the treatment of IOPD.

2. MATERIALS AND METHODS

2.1. Animals

The knock-in rat model for Pompe disease (Pompe or $Gaa^{-/-}$ rat) was generated using CRISPR/Cas9 technology. First, a specific RNA guide (gRNA; 3′-CCT GAC TTC TAC TCA CCA GG-5′) was designed to target the exon 7 of the rat *Gaa* gene. A single-stranded donor DNA sequence was designed to introduce the R385STOP nonsense mutation (C > T SNP) and a new *Bse*NI restriction site, to facilitate the genotyping of the offspring. Two silent mutations were introduced in the DNA donor to impair the re-binding of the gRNA or the re-cutting of Cas9. Moreover, two homology arms were also included in the donor DNA to enable homologous recombination with the rat *Gaa* genomic sequence. The gRNA, donor DNA, and Cas9 mRNA were microinjected into the pronucleus of one-cell Sprague–Dawley (SD) rat embryos. For the genotyping of the knock-in rats, common forward *Gaa*-Fw: 5′-CCA GAG CCC AAG AGT GTT GT-3′ and reverse *Gaa*-Rv: 5′- GTC TGG GAA GTC TGC AAA GC -3′ primers were used. A PCR reaction generated a 427 bp amplicon encompassing the point mutation, which was further digested with *Bse*NI restriction enzyme generating three fragments of 265, 107 and 55 bp in the WT allele, or three fragments of 171, 107 and 55 bp in the *Gaa* targeted allele. The resulting knock-in rats with the targeted allele were confirmed by Sanger sequencing of PCR amplicons using an ABI 3130xl genetic analyzer (ThermoFisher Scientific). Homozygous mutant rats ($Gaa^{-/-}$ or Pompe rats) were obtained by mating heterozygous littermates. Male rats were fed *ad libitum* with a standard diet (Teklad, Envigo) and maintained under a light–dark cycle of 12 h (lights on at 8:00 A.M.) and stable temperature (22 °C ± 2). Non-treated and AAV-treated rats were randomly divided into experimental groups. Wild-type littermate rats were used as a control. Sample size determination was based on previous experience with similar studies. All experimental procedures were carried out and reported following the Federation of Laboratory Animal Science Associations (FELASA) and ARRIVE guidelines, and the ethical and legal requirements from Generalitat de Catalunya, Spain, and the EU directives. All experimental procedures were approved by the Ethics Committee for Animal and Human Experimentation of the Universitat Autònoma Barcelona (UAB).

2.2. AAV vector production and administration

The AAVMYO3 expression cassette encoding GAA (Supplementary Fig. S1) was generated by cloning, between the ITRs (inverted terminal repeats) of AAV2, an optimized rat Acid alpha-glucosidase (r*Gaa*) coding sequence under the control of the synthetic muscle-specific promoter (SPc5-12)/CRE to enhance muscle-specific gene transcription, as previously described [32]. The AAVMYO3 muscle-tropic capsid was engineered via a semi-rational combination of DNA shuffling and peptide display to maximize gene delivery in skeletal and cardiac muscle as well as diaphragm [31]. AAVMYO3 vectors were produced by triple-transfection of HEK293 cells followed by a second-generation cesium chloride gradient-based purification method that renders vectors preparations devoid of empty capsids [41]. Viral vectors were determined by fluorescence using the Quant-iT™ PicoGreen™ dsDNA Assay Kit, as previously described [42]. For systemic administration, AAVMYO3 vectors were diluted in PBS supplemented with 0.001% F68 Pluronic® (Thermo Fisher Scientific) and injected via tail vein to male Pompe rats.

2.3. Sample collection

Rats were anesthetised by intraperitoneal injection (80 mg/kg ketamine and 10 mg/kg xylazine for rats). Animals were transcardially perfused with 100 mL of PBS to clear blood from tissues thus removing all traces of circulating GAA. Multiple peripheral tissues and the encephalon were dissected and either snap-frozen and stored at −80 °C or immersed in formalin for subsequent histological analysis.

2.4. Gene expression analysis

To determine *Gaa* expression, total RNA was obtained from several tissues with TriPure isolation reagent (Roche) using a RNeasy Mini Kit (Qiagen). Total RNA was reverse transcribed using the Transcriptor First Strand cDNA Synthesis kit (Roche). *Gaa* expression was assessed through real-time quantitative PCR (qRT-PCR) in a QuantStudio 5 Real-Time PCR System (ThermoFisher Scientific) using *Gaa* primers, which recognize both, endogenous *Gaa* and codon-optimized *Gaa*: Forward primer, 5′-GAC CTG GAC TAC ATG GAC GC-3'; reverse primer, 5′- AAG CCG TCC TGG TTG AA-3'. Values were normalized to the expression of the rat *Rplp0* gene, using forward primer, 5′-AAG CCA CAC TGC TGA ACA TG-3′ and reverse primer, 5′-TGC TGC CAT TGT CAA ACA CC-3′.

2.5. Enzyme activities

Tissue samples were mechanically disrupted (T10 Ultra-Turrax®, IKA®-Werke GmbH & Co.) and then sonicated in 600 μL of water. GAA and β-Hexosaminidase activity were determined in clarified supernatants using 4-methylumbelliferone-derived fluorogenic substrates. For GAA activity, 50 μg of protein diluted in 20 μL of water were incubated for 1 h at 37 °C with 40 μL of 4-methylumbelliferyl a-D-glucopyranoside (3 mM) (Sigma), diluted in acetate buffer solution (pH 4) (Sigma—Aldrich). The activity of β-hexosaminidase was measured in 0.4 μg of total protein with 20 μL of 4-methylumbelliferyl *N*-acetyl-β-D-glucosaminide (Sigma—Aldrich) for 1 h at 37 °C. After stopping both reactions by increasing the pH, released fluorescence (λ_{ex} 360 nm; λ_{em} 460 nm) was read with a Synergy HTX fluorimeter (Biotek Instruments). A standard curve was prepared using 4-methylumbelliferone, diluted in carbonate solution (pH 10.5). Enzyme activities were normalized against total protein content quantified by Bradford assay (Bio-Rad).

2.6. Glycogen content quantification

Glycogen content in skeletal muscles, diaphragm, heart, liver, brain and spinal cord samples was measured in perchloric extracts as previously described. Perchloric extracts were adjusted to pH 5 with 5 M K_2CO_3 and 10% $HClO_4$, and glycogen content was determined using the α-amyloglucosidase method [43]. Glucose was measured enzymatically (Glucose HK CP; Horiba Medical ABX Diagnostics) using a Pentra 400 Analyzer (Horiba Medical-ABX) and glycogen content was expressed as mg glucose per gram of tissue biopsies.

2.7. Vector genome copy number

Tissue samples were digested overnight at 56 °C in 300 μL of Tissue Lysis Solution supplemented with Proteinase K (0.2 mg/mL). Total DNA was isolated from supernatants with the MasterPureDNA Purification Kit (Lucigen). DNA was resuspended in distilled water and quantified using a Synergy HTX fluorimeter (Biotek Instruments). Vector genome copy numbers in 20 ng of total DNA were determined by quantitative PCR using the Light Cycler 480 Probes Master (Roche). Primers and probe were designed for a specific sequence within the optimized rat *Gaa* cDNA: forward primer, 5′-CTA CCG AGT GGA CCA GAA T-3′; reverse primer, 5′-CAT CTT CCA GAG CCA GGT AAA-3′; probe: 56-FAM/CTG GGA GCC/ZEN/ACA TCT CTG TTC CAC/3IABkFQ/. A reference standard curve was built from serial dilutions of a linearized plasmid bearing the SPc5-12 promoter and the optimized *Gaa* cDNA spiked into 20 ng/μL of non-transduced rat genomic DNA.

2.8. Western blot analyses

Quadriceps and diaphragm were mechanically homogenized in protein buffer (50 mM Tris—HCl, 0.27 M sucrose, 1 mM EDTA, 50 mM NaF, 10 mM Na β-glycerophosphate, 5 mM Ppi, 1% Triton X-100). Protein concentration was determined using the bicinchoninic acid (BCA) Protein Assay Kit (Thermo Fisher Scientific). SDS-PAGE was performed in an 8%—12% gradient polyacrylamide gel. After transfer, the membrane was blocked with BSA or nonfat dried milk and incubated with anti-LC3B (rabbit polyclonal; Novus Biologicals) and anti-p62 (rabbit polyclonal; Sigma—Aldrich) antibodies. Detection was performed using the corresponding horseradish peroxidase-labeled secondary antibodies and Western blotting detection reagent (ECL Plus; Amersham). LC3B-I, LC3B-II and p62 protein levels were normalized using Ponceau staining and densitometric quantification was performed using ImageJ software.

2.9. Histology and immunohistochemistry

Tissues were fixed for 12—24 h in 10% formalin, embedded in paraffin and sectioned. To determine skeletal muscle morphology, sections were stained with haematoxylin/eosin. Glycogen content was analysed by Periodic Acid Schiff (PAS) staining. Representative images were obtained with an Eclipse 90i microscope (Nikon). For LIMP2 immunohistochemistry, histological sections were incubated overnight at 4 °C with rabbit anti-LIMP2 (NB400; Novus Biologicals) primary antibody. Biotinylated Alexa Fluor® 568 anti-rabbit IgG (A11011; Invitrogen) or biotinylated goat anti-rabbit IgG (31820, Vector Laboratories) were used as secondary antibodies. For GFAP immunohistochemistry, histological sections were incubated overnight at 4 °C with rabbit anti-GFAP (Z0334, Dako Cytomation) as primary antibody and biotinylated goat anti-rabbit IgG (31820, Vector Laboratories) was used as secondary antibody. Hoechst (Sigma—Aldrich) was used for nuclear counterstaining of fluorescent specimens. Bright-field sections were stained with 3.3-diaminobenzidine (Sigma—Aldrich) and counterstained with haematoxylin. Images were obtained with a confocal Olympus Fluoview 1000 (Olympus Corp) or Leica SP5 (Leica Biosystems) microscope. NIS Elements Advanced Research 2.30 software was used to quantify LIMP2 and GFAP signal in 4 images per animal of each brain region using the same signal threshold settings for all

animals. The percentage area of each image that had positive signal was then calculated.

2.10. Electron microscopy

For transmission electron microscopy (TEM) analysis, rats were euthanized by intraperitoneal ketamine/xylazine overdose. A small portion ($\sim$1 mm^3) of each tissue was dissected and incubated at 4 °C for 2 h in 1 mL of 2.5% glutaraldehyde and 2% PFA as fixative. For semi-thin sections (800 nm), muscle samples were stained with toluidine blue dye and images were obtained with Nikon Eclipse 50i and 90i microscopes (Nikon). For TEM, samples were processed as previously described [44], and examined with a Hitachi H-7000 transmission electron microscope (Hitachi).

2.11. Naso-anal length measurement

Rats were positioned supine and the distance between the most rostral part of the head and the most caudal part of the abdomen (base of the tail) was measured.

2.12. Four-limb grip strength test

Grip strength was measured as maximum tensile force using a grid and recorded with a rat Grip Strength Meter (Panlab) equipped with a sensor capacity of 25 N and accuracy of 0.1%. The maximum of three pulls of the Grip Strength Meter was recorded and averaged.

2.13. Statistical analysis and data processing

Results are expressed as mean $\pm$ SEM. Statistical comparisons were made using either unpaired two-tailed *t*-test when comparing two groups or one-way analysis of variance (ANOVA) when comparing three groups. In ANOVA analysis, multiple comparisons between vehicle-treated Pompe rats and WT and AAV-*Gaa*-treated Pompe rats were made using Dunnett's post-test. Statistical significance was considered if $P < 0.05$. Kaplan—Meier curves were used to estimate survival and the log-rank test was used for comparisons.

3. RESULTS

3.1. Generation and characterization of a Pompe rat model

To overcome the limitations of the existing mouse models of PD, a knock-in (KI) Pompe rat model was generated using CRISPR/Cas9 technology. For targeted disruption of the rat *Gaa* gene, a single guide RNA (sgRNA) was designed to mediate the introduction of a specific inactivating point mutation (C > T SNP) in exon 7 (catalytic site) (Supplementary Fig. S2A). A donor DNA sequence that carried a nonsense mutation was designed to substitute an arginine-encoding codon for a STOP codon in the endogenous *Gaa* gene by homology-directed repair mechanisms (Supplementary Fig. S2A). Moreover, two silent mutations were introduced to modify the 3′ end of the sgRNA binding site and the PAM sequence to prevent inadvertent CRISPR/Cas9-mediated editing of the modified target site harboring the inactivating point mutation (C > T SNP) in exon 7. To facilitate the genotyping analysis and detection of positive KI rats, a *BseNI* restriction site was also introduced (Supplementary Fig. S2A). Afterwards, the specific sgRNA, the donor DNA, and the Cas9 mRNA were microinjected into one-cell rat embryos.

Successful targeting of the rat *Gaa* gene was confirmed by Sanger sequencing and PCR analysis (Supplementary Figs. S2B and C). Selective backcrosses, in two independent rat lines (L1 and L2), were performed during three generations between wild-type (WT) and heterozygous KI progenitor rats (F0) to segregate possible CRISPR/Cas9 off-target events [45,46]. Finally, homozygous KI *Gaa*$^{-/-}$ rats (Pompe rats) from L1 and L2 were obtained after crossing heterozygous *Gaa*$^{+/-}$ rats from F3. L1 and L2 Pompe rats showed undetectable levels of *Gaa* expression in all organs analyzed in both males (Supplementary Fig. S2D) and females (Supplementary Fig. S3A) and whole-body glycogen accumulation, especially in skeletal and cardiac muscles (Supplementary Fig. S2E and Supplementary Fig. S3B). Histological evaluation using Periodic acid Schiff (PAS) staining confirmed glycogen accumulation and revealed marked muscle pathology in male and female Pompe rats from both lines, mainly characterized by sarcoplasm vacuolization and fragmentation of myofibers (Supplementary Fig. S2F and Supplementary Fig. S3C). L1 and L2 Pompe rats from both genders also showed reduced body and muscle weight (Supplementary Figs. S2G and H; Supplementary Fig. S3D), severely impaired muscle function, evidenced by altered grip strength (Supplementary Fig. S2I and Supplementary Fig. S3E), as well as cardiomegaly and hepatomegaly (Supplementary Figs. S2J and K; Supplementary Figs. S3F and G), all key features of PD. Given that L1 and L2 male and female Pompe rats presented indistinguishable phenotypes, L2 male rats were selected for further characterization.

A decrease in body weight was already detected in 3-weeks-old male Pompe rats and it was progressively aggravated as animals aged (Figure 1A). Specifically, body weight of PD rats was reduced 13% at 3 weeks of age, decreasing to 25% and 40% in 20- and 33-weeks-old rats, respectively (Supplementary Fig. S4A). This phenotype is similar to human IOPD, as affected infants present failure to thrive, and are unable to gain weight and grow at the expected rate [1,47]. The reduction of body weight did not correlate with decreased naso-anal length at all ages analysed (Figure 1B; Supplementary Fig. S4B). Pompe rats showed hypotonia with decreased skeletal muscle mass (Supplementary Fig. S4C). These rats also presented a marked reduction of the median survival rate ($\sim$20 weeks) compared to WT rats (Figure 1C), with no PD rats surviving over 8 months of age, thus evidencing the severe phenotype of this new PD model.

3.2. Pompe rats develop early-onset skeletal muscle pathology

Pompe rats showed early and severe pathological accumulation of glycogen in all skeletal muscles, including diaphragm, which progressively increased with age (Figure 1D; Supplementary Fig. S5). In 4-weeks-old PD rats, numerous myofibers accumulated glycogen both in sarcoplasm and lysosomal-like vesicles (Supplementary Fig. S5). Glycogen storage in cytoplasm as a consequence of glycogen leakage out of lysosomes has been correlated with disease progression, severe myopathy and fibril dissolution in IOPD patients [48,49]. PD rats also showed early-onset myofiber degeneration, with slight sarcoplasm vacuolization already established at four weeks of age and fragmentation of sarcoplasm fully evident at 16 weeks of age (Figure 1E; Supplementary Fig. S6). Myofiber necrosis was also noted in 8-weeks-old PD rats (Figure 1E; Supplementary Fig. S6). Similar histopathological findings have been reported in IOPD patients [49—51]. Immunostaining against LIMP2 also evidenced a marked lysosomal distension already at 4 weeks of age (Supplementary Fig. S7A). Ultrastructural analysis by transmission electron microscopy (TEM) of quadriceps and diaphragm showed not only accumulation of glycogen in membrane-bound vesicles, compatible with glycogen-filled lysosomes, but also storage of granular glycogen disrupting the myofibrillar structure (Figure 1F; Supplementary Fig. S7B). Similar findings were made in PD patients [52]. Autophagic alterations were also detected in Pompe rats, including the presence of multivesicular bodies with undigested glycogen particles and other secondary storage materials or cellular debris and classical double-membrane autophagosomes (Figure 1G; Supplementary Fig. S7B). The early onset of the

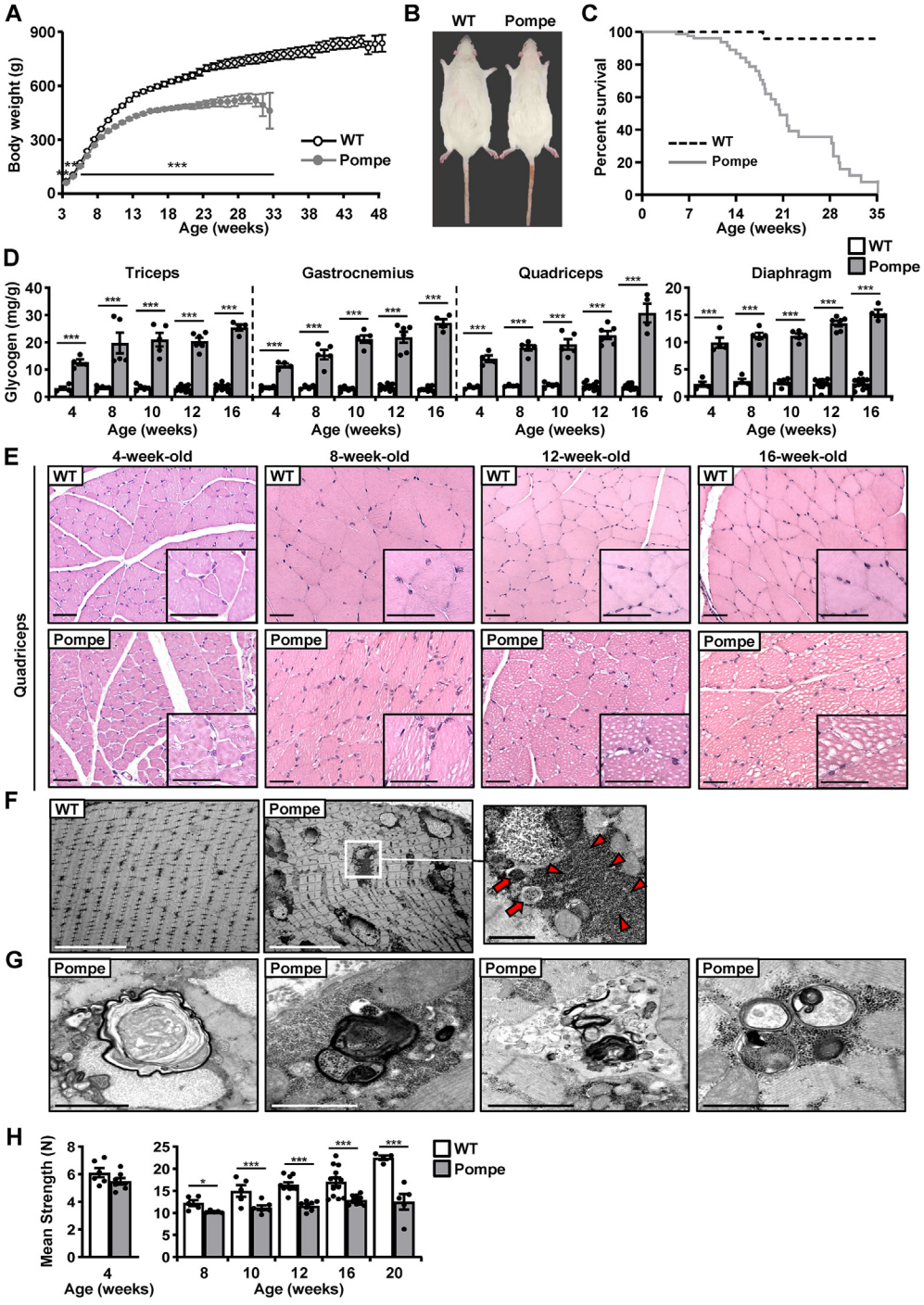

Figure 1: The novel Pompe rat model developed a severe, early-onset and progressive muscular pathology. (A) Body weight follow-up of WT (n = 161) and Pompe (n = 112) rats. Pompe rats showed reduced body weight values compared with WT counterparts. (B) Representative image of 20-weeks-old WT and Pompe rats. (C) Kaplan–Meier survival analysis of WT (n = 157) and Pompe rats (n = 100). Pompe rats showed a shorter lifespan, with a mean survival of ~20 weeks, compared with WT rats. (D) Quantification of glycogen content in triceps, gastrocnemius, quadriceps and diaphragm from 4-, 8-, 10-, 12- and 16-weeks-old WT and Pompe rats (n = 2–11 animals/group). Results are expressed as mg glucose per g of tissue weight. (E) Histological analysis of quadriceps sections stained with hematoxylin/eosin from 4-, 8-, 12- and 16-weeks-old WT and Pompe rats. Insets reveal progressive vacuolization of sarcoplasm from Pompe muscle fibers with age. Scale bars, 50 μm. (F) Ultrastructural analysis by TEM of quadriceps from 20-weeks-old WT and Pompe rats revealed large accumulation of electrodense material in muscle fibers, compatible with glycogen particles. Both free glycogen particles (arrowheads) and lysosomes filled with them (arrows) were observed. Scale bars, 5 μm. (G) Electron-micrographs evidenced autophagic alterations by formation of double membrane sequestering vesicles, multivesicular bodies and accumulation of secondary electrolucent storage materials. (H) Grip strength analysis of 4-, 8-, 10-, 12-, 16- and 20-weeks-old WT and Pompe rats (n = 5–29 animals/group). Pompe rats exhibited reduced muscular strength compared to WT counterparts. Results are shown as mean ± SEM. Unpaired two-tailed Student's t-test, except in panel (C), where Kaplan–Meier curves were used to estimate survival and the log-rank test was used for comparisons. $*P < 0.05$; $**P < 0.01$; $***P < 0.001$ *vs* WT.

muscle pathology resulted in reduced muscle strength, which was already detected in 4-weeks-old animals and worsened as animals aged (Figure 1H). Altogether, this rat model of PD recapitulates the severe and early myopathy characteristic of human IOPD.

3.3. Pompe rats present severe cardiac alterations and hepatomegaly

The clinical phenotype of IOPD is mainly characterized by cardiomyopathy, caused by glycogen storage in the heart. Concurrent with diaphragm alterations, the severe cardiomegaly detected in human IOPD patients exacerbates the cardiopulmonary complications that lead to death during the first year of life [53]. Pompe rats developed early-onset cardiomegaly characterized by progressive accumulation of glycogen (Figure 2A,B). Histological analysis of heart sections stained with PAS further confirmed that glycogen accumulation was progressively increased in cardiomyocytes as the animals aged (Figure 2C), thus demonstrating quick establishment of myocardial alterations in this new rat model of PD. TEM analysis further evidenced the presence of large numbers of electrodense storage vesicles in cardiomyocytes (Figure 2D), which was similar to the glycogen accumulation detected in skeletal muscle fibers (Figure 1F,G; Supplementary Fig. S7B).

Hepatomegaly is a clinical feature of IOPD [53]. Pompe rats showed signs of hepatomegaly at the age of four weeks and older although liver glycogen content only slightly increased in these animals (Supplementary Figs. S8A and B). Neither histological alterations nor significant differences in PAS staining were detected in liver sections from affected rats compared with wild-type animals (Supplementary Fig. S8C).

3.4. Glycogen storage in CNS of Pompe rats

It has also been described that glycogen accumulates in the central nervous system (CNS) of PD patients [2,3]. Similarly, progressive accumulation of glycogen was also detected in brain and spinal cord (SC) as Pompe rats aged (Figure 3A and Supplementary Fig. S9A). CNS glycogen levels were much lower (~10-fold) than those detected in skeletal and cardiac muscles (Figure 1D, Figure 2B, Figure 3A and Supplementary Fig. S9A). PAS-staining of brain and SC sections from Pompe rats evidenced widespread glycogen accumulation. In brain, increased glycogen storage was mainly detected in medulla, pons, midbrain, cerebellum and cerebral cortex, particularly in neurons, Purkinje, Bergman and glial cells (Figure 3B–F). In SC, accumulation of glycogen was observed in sensitive neurons, motor neurons and radial glial cells of Pompe rats (Supplementary Figs. S9B and C). Consistent with the elevated accumulation of glycogen, increased LIMP2^{+} area was revealed in all regions of brain analysed (Supplementary Figs. S10A and B). Moreover, marked astrocytosis was detected in brain, indicating that glycogen storage also caused a neuroinflammatory response in PD rats (Supplementary Figs. S10C and D). Therefore, Pompe rats presented CNS pathology mimicking the glycogen storage disease detected in human PD patients [4].

3.5. Systemic administration of a novel muscle-specific AAVMYO3-*Gaa* gene therapy reverted skeletal muscle pathology of Pompe rats

We next evaluated the therapeutic benefit of an innovative AAV-mediated gene therapy approach based on the use of a novel engineered muscle-tropic AAVMYO3 capsid to enhance muscle transduction in conjunction with a muscle-targeted promoter/CRE for robust expression in skeletal muscles, diaphragm, and heart [31,32]. Four-weeks-old male Pompe rats were systemically administered with either vehicle or 5×10^{13} viral genomes (vg)/kg of AAVMYO3 vectors encoding rat *Gaa* under the control of the Spc5-12 promoter/CRE (AAV-*Gaa*). As previously shown (Figure 1A), non-treated Pompe rats showed progressive reduction of body weight, while rats treated with AAV-*Gaa* maintained body weight gains similar to WT rats (Figure 4A). Treated PD rats showed normal survival at 20 weeks of age compared to the non-treated PD rat cohort, in which about 40% of animals had to be euthanized (Supplementary Fig. S11A).

Treatment of Pompe rats with AAV-*Gaa* vectors led to widespread and efficient vector biodistribution (viral genomes/diploid genome; vg/dg) throughout the entire muscular system, while completely detargeting liver (Figure 4B). AAV-*Gaa* vector genomes were neither detected in CNS (Figure 4B). AAV-*Gaa* administration resulted in increased *Gaa* expression and activity (~2- to 4-fold *vs.* WT) in all muscles analyzed, including diaphragm and heart, compared to non-treated Pompe rats (Figure 4C,D). *Gaa* expression and enzyme activity were not significantly higher than background levels in other tissues, such as liver, brain and SC, also involved in PD pathology (Figure 4E,F; Supplementary Fig. S11B). In skeletal and cardiac muscles, the high levels of GAA activity led to a complete normalization of the glycogen storage pathology (Figure 4G). No correction of glycogen content was observed in liver, brain and SC (Figure 4H; Supplementary Fig. S11C). AAV-*Gaa*-treated Pompe rats showed complete reversal of cardiomegaly, as well as full recovery of skeletal muscle mass and strength, indistinguishable from wild-type (Figure 4I,J). Histological analysis confirmed correction of muscular pathology, as Pompe rats treated with AAV-*Gaa* vectors showed complete clearance of glycogen content and no signs of sarcoplasm disruption in all striated muscles analysed (Figure 5A; Supplementary Fig. S11D). TEM analysis of quadriceps, diaphragm and heart of treated-Pompe rats further evidenced that ultrastructural morphology of striated muscles was indistinguishable from WT rats, with lack of glycogen-filled lysosomes and absence of granular glycogen disrupting the myofibrillar structure (Figure 5B). Moreover, immunostaining against LIMP2 of triceps sections confirmed lack of lysosomal distension after AAV-*Gaa* treatment (Figure 6A).

3.6. Treatment with AAVMYO3-*Gaa* normalized autophagy and lysosomal homeostasis

Lysosomal dysfunction has been linked to severe autophagy impairment and accumulation of autophagic vacuoles and debris in skeletal muscles of PD patients [52]. Treatment of Pompe rats with AAV-*Gaa* vectors counteracted autophagosome formation as revealed by normalization in quadriceps and diaphragm of key proteins in autophagic flux, such as LC3B-I, LC3B-II and p62 [54–56] (Figure 6B,C). This treatment also corrected the disrupted lysosomal homeostasis, a feature of lysosomal storage disorders [57,58], by normalizing β-hexosaminidase activity in skeletal and cardiac muscles of Pompe rats (Figure 6D).

4. DISCUSSION

Pompe disease is a severe metabolic disease with no cure. Although an enzyme replacement therapy (ERT) is already approved for PD, significant drawbacks greatly limit its therapeutic efficacy, such as incomplete correction of muscle pathology, need of multiple weekly injections and high cost [8]. In this work, we reported the generation of a new rat model of PD using CRISPR/Cas9 technology, which closely recapitulates many of the severe alterations observed in human IOPD. Next, using an AAV vector designed to efficiently target expression of GAA in muscle, while avoiding liver transduction, we showed complete rescue of the glycogen metabolism alterations in muscle, resulting in

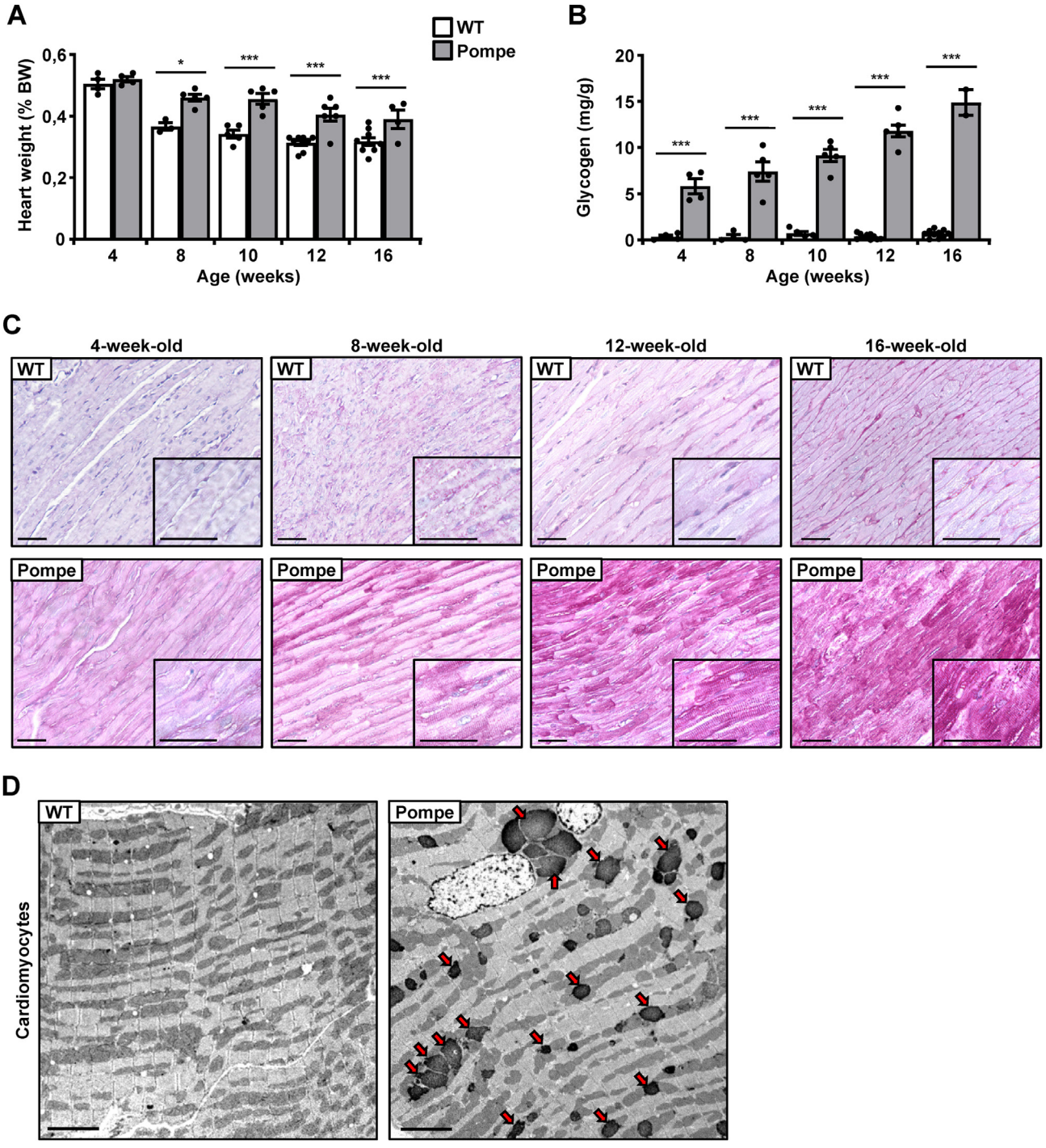

Figure 2: Pompe rats developed the hypertrophic cardiomyopathy as in human IOPD. (A) Heart weight of 4-, 8-, 10-, 12- and 16-weeks-old WT and Pompe rats (n = 4–9 animals/group). Pompe rats showed increased heart weight, which corresponded to a marked cardiomegaly. Results are expressed as percentage of body weight (% BW). (B) Quantification of glycogen content in heart from 4-, 8-, 10-, 12- and 16-weeks-old WT and Pompe rats (n = 2–11 animals/group). Results are expressed as mg glucose per g of tissue weight. (C) Histological analysis of heart sections stained with PAS from 4-, 8-, 12- and 16-weeks-old WT and Pompe rats. Images revealed progressive glycogen accumulation in Pompe hearts with age. Scale bars, 50 μm. (D) Ultrastructural analysis by TEM of heart revealed wide accumulation of electrodense material (arrows), compatible with glycogen particles, only in cardiomyocytes from 20-weeks-old Pompe rats. Scale bars, 10 μm. Results are shown as mean ± SEM. Unpaired two-tailed Student's t-test. $^{*}P < 0.05$ and $^{***}P < 0.001$ *vs* WT.

normalization of muscle morphology and function, and survival of affected PD animals.

Translation of preclinical results into clinical trials has been challenging, owing in part to the limited ability of animal models to recapitulate disease features seen in humans. The rat model described here represents an important milestone in the development of a severe PD model. This rat model developed the severe myopathy of human IOPD, with an early-onset and progressive muscle pathology, mainly

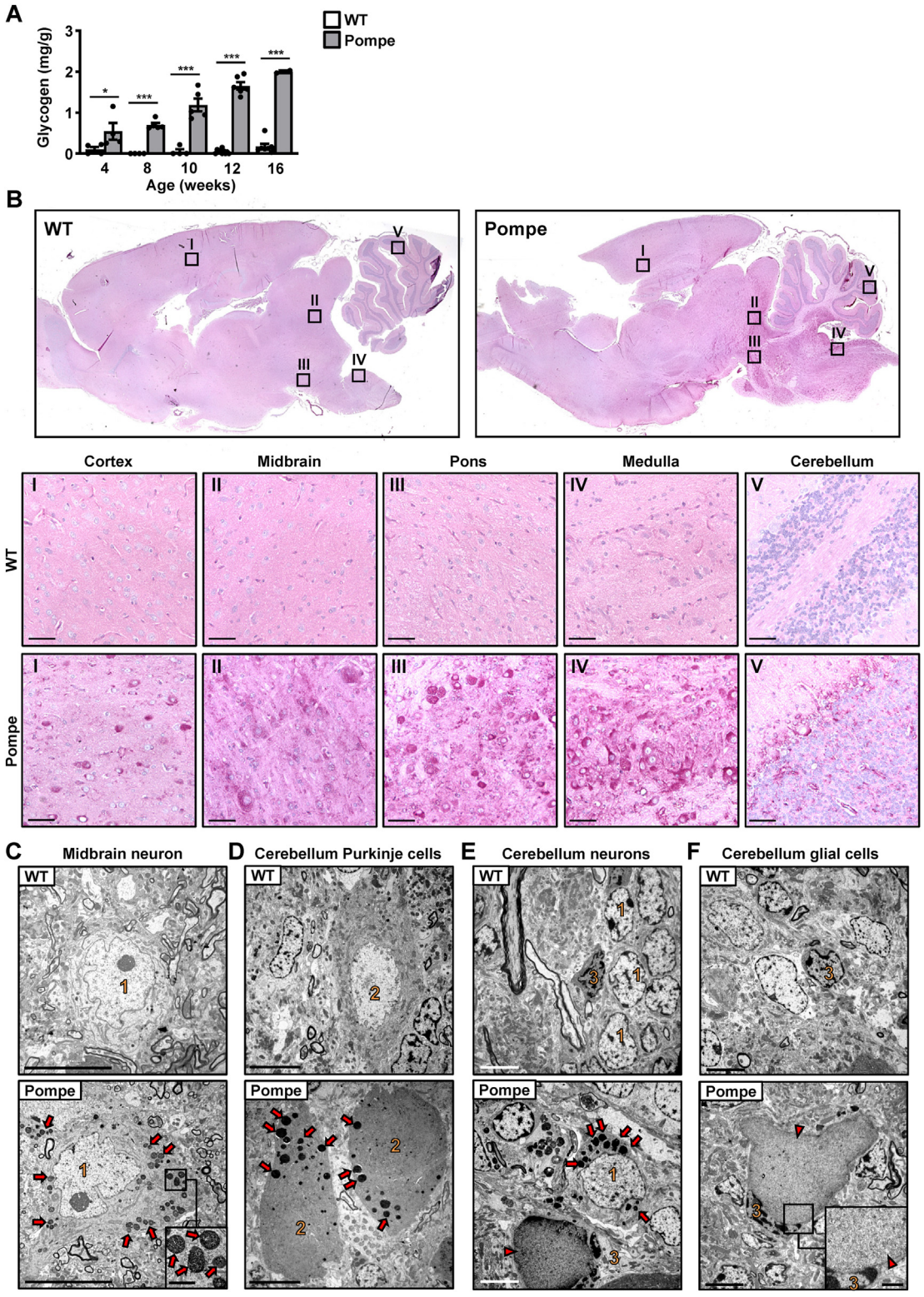

Figure 3: Evaluation of glycogen storage in brain of Pompe rats. (A) Quantification of glycogen content in brain from 4-, 8-, 10-, 12- and 16-weeks-old WT and Pompe rats (n = 2–10 animals/group). Results are expressed as mg glucose per g of tissue weight. (B) Histological analysis of brain sections stained with PAS from 16-weeks-old WT and Pompe rats. Brain sections from Pompe rats showed widespread glycogen accumulation, especially in caudal regions. Insets of different brain areas (panel I to V) revealed glycogen accumulation especially in medulla and pons regions. Scale bars, 50 μm. (C-F) Ultrastructural analysis of midbrain and cerebellum from 20-weeks-old WT and Pompe rats. TEM analysis in *Gaa*-deficient rats revealed neurons and Purkinje cells with many electrodense vesicles (arrows) in the cytoplasm, compatible with glycogen particles, and the presence of extremely large vesicles filled with storage materials with different densities (arrowhead) in glial cells. Scale bars, 10 μm (C, E, F) and 20 μm (D); inset, 2 μm (C, F). Neurons (1), Purkinje cells (2), glial cells (3). Results are shown as mean ± SEM. Unpaired two-tailed Student's t-test. $^{*}P < 0.05$ and $^{***}P < 0.001$ *vs* WT.

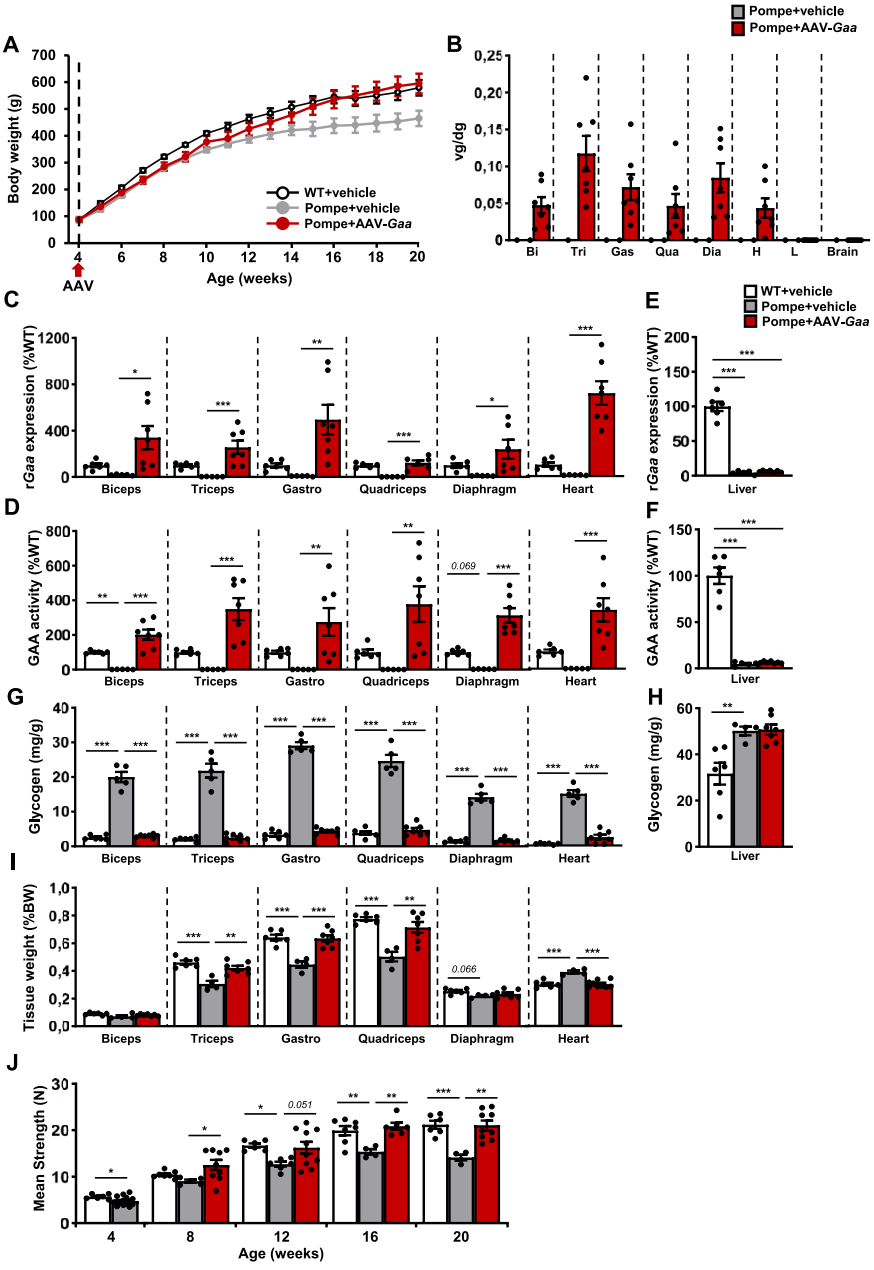

Figure 4: Treatment with the novel AAVMYO3-*Gaa* vector completely counteracted the severe muscular pathology of Pompe rats. Analysis of 20-weeks-old WT (n = 7) and Pompe rats treated with empty vehicle (n = 6) or AAV-*Gaa* vectors (n = 10) at four weeks of age. (A) Body weight follow-up. Treatment with AAV-*Gaa* led to normalization of body weight compared with vehicle-treated Pompe rats. (B) Vector genome copy number analysis showed efficient transduction of skeletal muscles and heart. No viral genomes were detected in non-targeted organs, such as liver and brain. (C) Expression analysis of r*Gaa* in skeletal muscles and heart. A marked increase of r*Gaa* expression was detected 16 weeks after AAV-*Gaa* vector administration. Gastro, gastrocnemius. Results of r*Gaa* expression are expressed as % of WT. (D) GAA activity in skeletal muscles and heart. AAV-*Gaa*-treated Pompe rats showed higher levels of GAA activity than WT rats. WT GAA activity was set to 100%, corresponding to 11.42 ± 0.41 (biceps), 12.02 ± 0.76 (triceps), 11.10 ± 0.98 (gastrocnemius), 9.48 ± 1.45 (quadriceps), 17.21 ± 1.20 (diaphragm) and 23.62 ± 2.40 (heart) nmol/h/mg. (E) Expression analysis of r*Gaa* in liver. r*Gaa* expression was undetectable in vehicle-treated and AAV-*Gaa*-treated Pompe rats in both tissues. Results of r*Gaa* expression are expressed as % of WT. (F) GAA activity in liver. Residual GAA activity was detected in vehicle-treated and AAV-*Gaa*-treated Pompe rats compared to WT rats. Liver WT GAA activity was set to 100%, corresponding to 18.04 ± 0.46 nmol/h/mg. (G) Quantification of glycogen content in skeletal muscles and heart. A complete correction of glycogen accumulation was detected after AAV-*Gaa* administration to Pompe rats. Results are expressed as mg glucose per g of tissue weight. (H) Quantification of glycogen content in liver. Similar glycogen accumulation was detected between vehicle-treated and AAV-*Gaa*-treated Pompe rats. Results are expressed as mg glucose per g of tissue weight. (I) Tissue weight analysis of heart and skeletal muscles. AAV-*Gaa* treatment counteracted cardiomegaly and hypotonia of vehicle-treated Pompe rats. Results are expressed as percentage of body weight (%BW). (J) Grip strength analysis of 4-, 8-, 12-, 16- and 20-weeks-old WT, vehicle-treated and AAV-*Gaa*-treated Pompe rats. AAV-*Gaa* treatment normalized muscular strength (n = 4–10 animals/group). Results are shown as mean ± SEM. One-way ANOVA, Dunnett's post-test except in (B), where unpaired two-tailed Student's t-test was used. $^{*}P < 0.05$; $^{**}P < 0.01$ and $^{***}P < 0.001$ *vs* vehicle-treated Pompe rats.

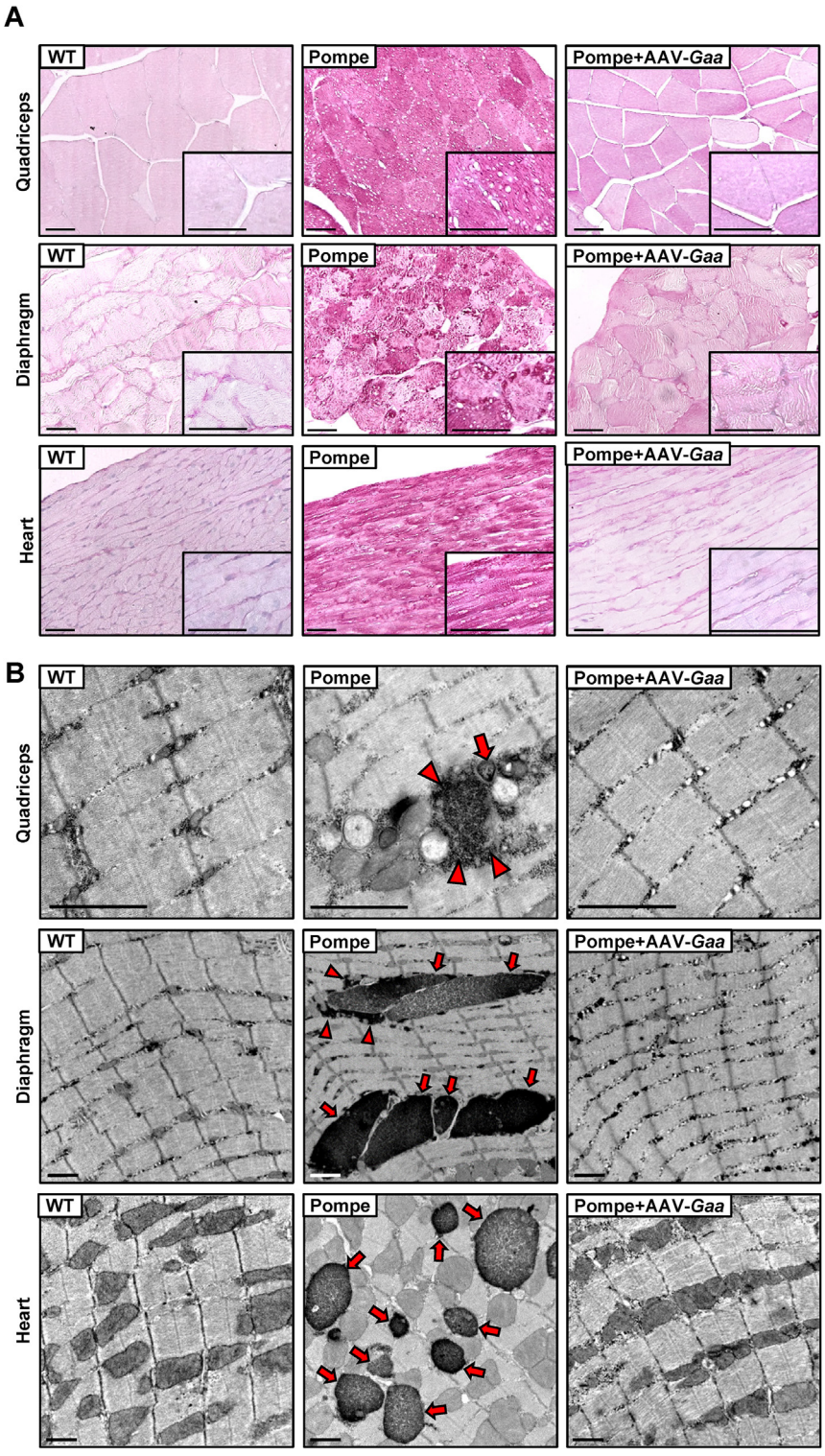

Figure 5: Correction of glycogen storage pathology in skeletal and cardiac muscle fibers of AAVMYO3-*Gaa*-treated Pompe rats. (A) Histological analysis of quadriceps, diaphragm and heart sections stained with PAS from 20-weeks-old WT, vehicle-treated and AAV-*Gaa*-treated rats. PAS staining revealed vacuolization and massive glycogen accumulation in myofibers from vehicle-treated Pompe rats. In contrast, AAV-*Gaa*-treated Pompe rats showed complete normalization of glycogen accumulation without any cytoplasmic vacuolization. Scale bars, 50 μm. (B) Ultrastructural analysis by TEM of quadriceps, diaphragm and heart from 20-weeks-old male WT, vehicle-treated and AAV-*Gaa*-treated Pompe rats. In contrast to vehicle-treated Pompe rats, a complete clearance of glycogen granules (arrowheads) and electrodense storage vesicles (arrows) was detected in AAV-*Gaa*-treated Pompe rats, indistinguishable from healthy littermates. Scale bars, 2 μm.

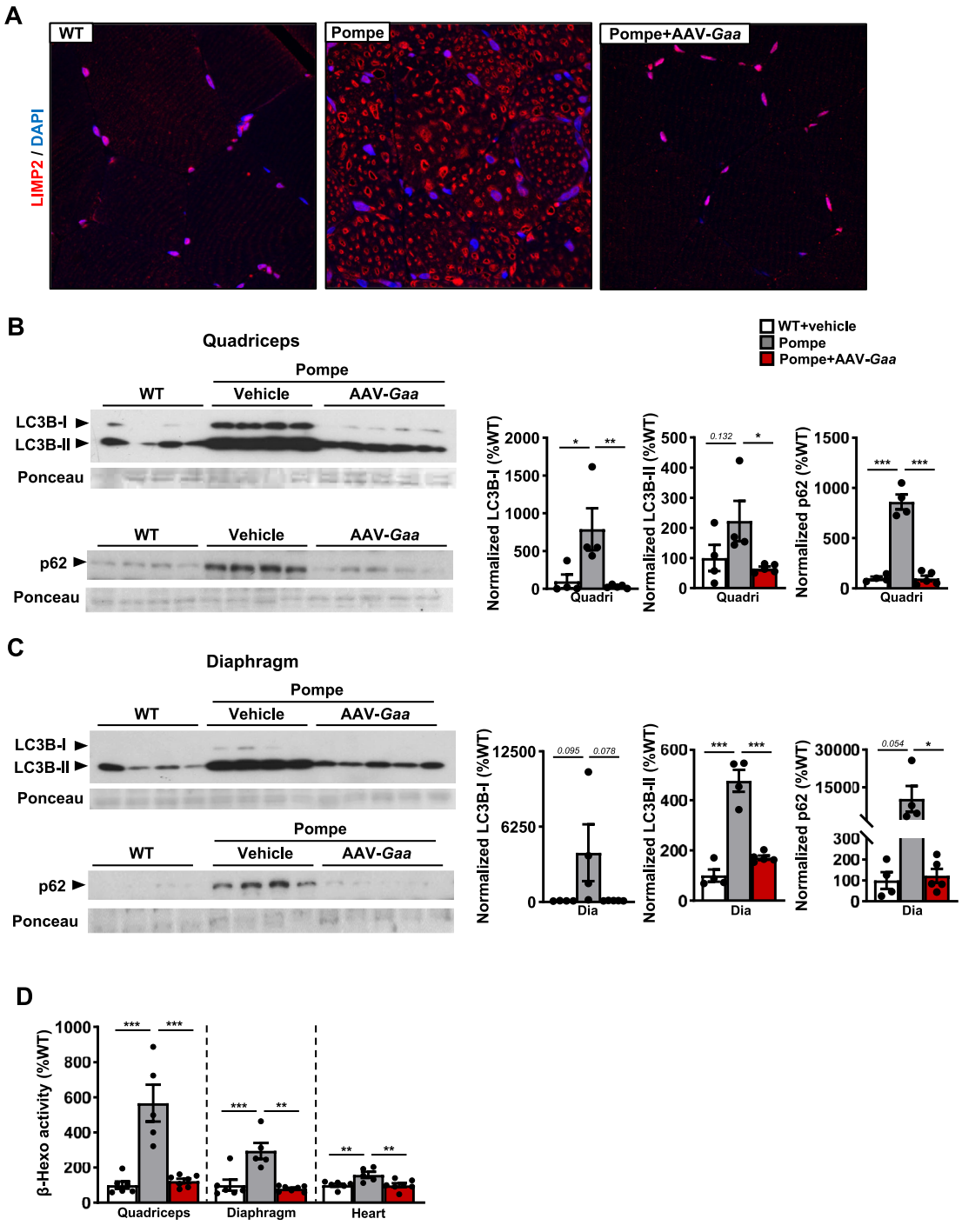

Figure 6: Treatment with the AAVMYO3-*Gaa* vector corrected autophagy flux and lysosomal homeostasis in Pompe rats. (A) LIMP2 immunohistochemistry of triceps sections from 20-weeks-old WT, vehicle-treated and AAV-*Gaa*-treated rats. Pompe skeletal muscle fibers showed increased numbers of lysosomes and lysosomal distension. In contrast, AAV-*Gaa*-treated Pompe myofibers were indistinguishable from healthy WT littermates. Magnification, 63×. (B,C) Representative immunoblots of a Western blot analysis of LC3B-I, LC3B-II and p62 proteins in quadriceps (B) and diaphragm (C) from 20-weeks-old WT, vehicle-treated and AAV-*Gaa*-treated Pompe rats (n = 4–5). Histograms depict the densitometric quantification analysis using two different immunoblots, one for LC3B-I and LC3B-II protein and the other for p62, which were normalized using Ponceau staining. Pompe rats showed higher presence of LC3B-I, LC3B-II and p62 proteins. Treatment with AAV-*Gaa* vectors normalized alterations in the autophagic flux. (D) β-hexosaminidase (β-Hexo) activity in quadriceps, diaphragm and heart from 20-weeks-old WT (n = 6), vehicle-treated (n = 5) and AAV-*Gaa*-treated (n = 7) Pompe rats. While vehicle-treated Pompe rats showed increased levels of β-hexosaminidase activity, treatment with AAV-*Gaa* vectors showed indistinguishable levels of β-hexosaminidase activity compared to WT rats. WT β-hexosaminidase activity was set to 100%, corresponding to 49.59 ± 10.32 (quadriceps), 134.28 ± 41.77 (diaphragm) and 236.39 ± 20.06 (heart) nmol/h/mg. Results are shown as mean ± SEM. One-way ANOVA, Dunnett's post-test. $^{*}P < 0.05$; $^{**}P < 0.01$ and $^{***}P < 0.001$ *vs* vehicle-treated Pompe rats.

characterized by marked glycogen accumulation, widespread hypotonia and impaired muscle function [47,59–61]. Pompe rats also presented hypertrophic cardiomyopathy and hepatomegaly at young ages [47,59–61]. Moreover, the novel PD rat model showed glycogen accumulation in brain and SC, as observed in human PD [4,7]. Given the quick progression of the disease, Pompe rats showed a marked reduction of mean and maximum lifespan, with no PD rats surviving over 8 months of age. Therefore, PD rats showed the lowest survival rate achieved in comparison with any existing PD mouse model [13–16,20,21,33–40]. To date, seven different PD mouse models have been generated [15,33–37,39,40]. All of them accumulated glycogen in the heart and skeletal muscles but showed variable disease severity. The $6^{neo}/6^{neo}$ mice develop early-onset myopathy and severely impaired muscle function [33], being the most used PD animal model for pre-clinical therapy development over the past 25 years. Nevertheless, $6^{neo}/6^{neo}$ mice develop critical features of both the infantile and adult forms of the human Pompe disease [13,15,16,21,33,62]. The Gaa $KO^{DBA2/J}$ mice showed early-onset spinal cord and respiratory defects but no striking differences in muscle disease and strength compared to $6^{neo}/6^{neo}$ mice [15]. Two knock-in PD mouse models exhibited skeletal and cardiac muscle pathology but did not display premature mortality [39,40]. Importantly, one advantage of rat models is their close physiological similarity to humans [63,64]. Similar to the observations made in Pompe rats, rat models of other genetic disorders, including diseases with muscular involvement, also showed disease phenotypes that more closely recapitulate the pathological clinical features of the human disease [65–69]. Rat models have also been shown to be more suitable than mice in dose-finding gene transfer studies [70,71].

In vivo AAV-mediated gene therapy offers the possibility of a one-time treatment, with the prospect of lifelong beneficial effects. To this aim, production of a number of therapeutic proteins for extended periods of time has been documented in several animal models and human studies [72–77]. Similarly, several AAV-mediated gene therapy strategies have been proposed for the treatment of PD, with several ongoing clinical trials for LOPD (NCT03533673, NCT02240407, NCT04174105, NCT04093349). In one completed clinical trial for IOPD (NCT00976352), an AAV1 vector encoding for GAA was administered intraparenchymally into the diaphragm. Although significant reduction of accumulated glycogen and improved *in vivo* ventilatory capacity were achieved, therapeutic benefit was restricted to diaphragm due to local delivery of the AAV vector [38,78].

Two clinical trials for LOPD are based on liver gene transfer (NCT03533673 and NCT04093349). Liver-mediated gene therapy approaches target the liver and use it as a secretory pump of therapeutic GAA to the main circulation with the aim of cross-correcting the afflicted muscles [13,15,17]. Despite showing promising results at preclinical level [13,15], the potential therapeutic efficacy of liver-mediated gene transfer is limited by the episomal nature of the AAV genomes, which tend to be diluted upon hepatocyte cell division, resulting in short-lived transgene expression in neonate animals [14,25,79–81]. While strategies to allow for vector readministration are being explored [82–84], the development of high-titer, long lasting anti-AAV antibodies post vector delivery [85] currently prevent redosing of AAV. Indeed, from a total of 32 ongoing clinical trials for liver-directed gene therapy of inborn errors of metabolism, 27 trials enroll >18-years-old patients [26].

Direct gene transfer to muscle is a potential strategy to achieve long-term gene expression in children. The approach has been explored preclinically in PD [14,22,86–89] and in the clinic in the context of Duchenne muscular dystrophy (DMD) [90] and X-linked myotubular myopathy (XLMTM) (NCT03199469). Preclinically, systemic administration of naturally occurring serotypes such as AAV6, 7, 8 and 9 and new synthetic AAV engineered capsids has been used to target the muscle and heart [10,14,18–23,28–31,87,88,91,92]. Nevertheless, PD mice treated with most of these vectors, even with very high doses, did not achieve transduction of the whole muscular system and showed partial clearance of glycogen content in affected skeletal muscles, in contrast to the results obtained in PD rats treated with AAVMYO3-*Gaa* vectors [10,14,18–22,87,88,91]. Similarly, intravenous administration to adult PD mice of AAV8 vectors expressing human GAA specifically in skeletal muscle and heart (AT845) normalized glycogen levels in cardiac and skeletal muscles, and grip response [23]. Nevertheless, a dose 6-fold higher (3×10^{14} vg/kg) than the one used in PD rats was required to achieve full therapeutic efficacy, which resulted in high levels of transduction in off target tissues, mainly the liver [23]. Moreover, survival of the PD mice treated with AT845 vectors was not reported [23].

Currently, newborn screening programs for PD allow for early detection and very early intervention (within days after birth) in patients with IOPD [5,93]. Therapeutic efficacy persistence was obtained in PD rats treated with AAVMYO3-GAA vectors although the animals were treated at a very early age. Similar to the results obtained in PD rats, AAV-mediated gene transfer of GAA to muscle of neonate PD mice also resulted in persistent therapeutic outcomes [14,22,87,88]. Additional studies in fetal rhesus monkeys [89] and PD mice [86] treated with AAV vectors showed persistent expression of GAA in muscle but not liver. Moreover, IOPD patients and PD mice display inefficient muscle regeneration, likely due to poor satellite cell activation but not altered number of satellite cells [94–98]. Likewise, no signs of myofiber regeneration and/or central nuclei were observed in PD rats at any age analysed. Therefore, these results suggest that muscle growth seems to have a lower effect on AAV genome dilution than the liver. Nevertheless, therapeutic AAV genomes may potentially be diluted in the muscles of paediatric IOPD patients as they age, especially in newborn-treated IOPD patients. Future clinical muscle-directed AAV-based studies may provide insights on whether sustained therapeutic benefit observed in preclinical models is maintained in paediatric IOPD patients.

In the clinical setting, mild to severe toxicities have been documented following systemic AAV-mediated gene transfer. These include complement-related and liver toxicities, leading in some cases to fatalities [27,99–102] and, in preclinical models, dorsal root ganglia (DRG) toxicities [103,104]. Similarly, treatment of non-human primates with AT845 at doses $\geq 2 \times 10^{14}$ vg/kg resulted in presence of mononuclear-to-mixed cell infiltrates in the liver and degeneration of DRG neurons, even when using the species-specific *Gaa* transgene [23]. A phase I/II clinical trial aimed at assessing safety and efficacy of AT845 in LOPD patients is currently ongoing (NCT04174105). The trial was recently placed on hold by FDA due to potential DRG toxicities.

The work presented here represents the first example of a strategy to develop a safe and effective gene therapy to deliver *Gaa* to muscle for IOPD. We first utilized a bioengineered AAV variant (AAVMYO3) able to transduce the muscle at levels higher than the gold standard AAV8 and AAV9 vectors while detargeting liver [31], thus avoiding hepatoxicity. Moreover, seroprevalence of the AAVMYO3 capsid in human subjects is comparable to AAV9, indicating that the serologic profile of the AAVMYO3 capsid is compatible with clinical translation [31]. Next, to optimize the *Gaa* transgene expression cassette we employed a muscle-specific promoter in conjunction with a transcriptional *cis*-regulatory element (CRE) [32]. The high transduction efficiency achieved after systemic administration to Pompe rats resulted from

combining the AAVMYO3 capsid with the muscle-targeted promoter, leading to widespread expression of *Gaa* in skeletal muscle throughout the body. The AAVMYO3-*Gaa* vector demonstrated breakthrough therapeutic efficacy by (1) increasing the levels of GAA activity in cardiac and skeletal muscles, (2) normalizing glycogen metabolism and storage pathology, (3) restoring muscle mass and strength, (4) counteracting cardiomegaly and (5) normalizing survival rate.

Recent studies elucidate an important CNS involvement in PD [4,7]. Abnormal glycogen accumulation in the cerebral cortex, midbrain, pons, medulla, cranial nerve nuclei, brainstem, cerebellum, and SC as well as astrogliosis have been reported in PD patients [4]. Similarly, accumulation of glycogen in the brain and spinal cord and neuroinflammation were detected in PD rats and PD mouse models [4,13,15]. The lack of targeting of CNS is one of the limitations of our work and perhaps it could be addressed in the future by 1) further evolving the AAV platform to add more CNS tropism; 2) combining muscle with CNS-targeted promoter/enhancer elements [14].

Altogether, this work supports the clinical translation of this muscle-specific strategy based on engineered AAV vectors as a new therapeutic option not only for human PD, but also for other inherited muscle diseases, such as Duchenne Muscular Dystrophy (DMD) and XLMTM, which also can be limited by the inefficient widespread delivery of therapeutic transgenes throughout the muscular system. Moreover, liver detargeted properties of our engineered AAV vectors would prevent hepatotoxicities. These results open a new window to safer gene therapy approaches for diseases with muscular involvement, enabling the use of lower doses that achieve high and widespread transduction efficiency.

CREDIT AUTHORSHIP CONTRIBUTION STATEMENT

Sergio Muñoz: Conceptualization, Formal analysis, Investigation, Visualization, Writing — original draft, Writing — review & editing. **Joan Bertolin:** Conceptualization, Formal analysis, Investigation, Visualization, Writing — original draft. **Veronica Jimenez:** Conceptualization, Investigation, Supervision, Writing — original draft, Writing — review & editing. **Maria Luisa Jaén:** Data curation. **Miquel Garcia:** Data curation. **Anna Pujol:** Methodology, Resources. **Laia Vilà:** Data curation. **Victor Sacristan:** Data curation. **Elena Barbon:** Methodology, Resources. **Giuseppe Ronzitti:** Methodology, Resources. **Jihad El Andari:** Methodology, Resources. **Warut Tulalamba:** Methodology, Resources. **Quang Hong Pham:** Methodology, Resources. **Jesus Ruberte:** Data curation. **Thierry VandenDriessche:** Funding acquisition, Writing — review & editing. **Marinee K. Chuah:** Funding acquisition, Writing — review & editing. **Dirk Grimm:** Funding acquisition, Writing — review & editing. **Federico Mingozzi:** Conceptualization, Funding acquisition, Writing — review & editing. **Fatima Bosch:** Conceptualization, Funding acquisition, Investigation, Supervision, Writing — original draft, Writing — review & editing.

ACKNOWLEDGEMENTS

We thank J. Barrero, L. Hernández, M. Moya, Á. Vázquez, L. Noya and S. Frankhauser for technical assistance. We kindly acknowledge the support provided by the MYOCURE project to F.B., M.K.C., T.V., D.G. and F.M. MYOCURE has received funding from the European Union's Horizon 2020 research and innovation programme under grant agreement No. 667751. F.B. received support from MCIN/AEI/10.13039/501100011033 (PID2020-113864RB-100), from Generalitat de Catalunya (2021 SGR 01012, ICREA Academia Award to F.B.) and from CIBER-Consorcio Centro de Investigación Biomédica en Red- (CB07/08/0037), Instituto de Salud Carlos III, Ministerio de Ciencia e Innovación. V.S. was recipient of a predoctoral fellowship (Grant FPU2014-FPU14/05268) funded by MCIN/AEI/10.13039/501100011033 and "ERDF A way of making Europe". T.V. and M.K.C. received grant support from the Vrije Universiteit Brussel Industrieel Onderzoeksfonds (IOF) Groups of Expertise in Advanced Research (GEAR) and Strategic Research Project (SRP Grower), F.W.O. (Fonds Wetenschappelijk Onderzoek Vlaanderen), Koning Boudewijnstichting (Fonds Walter Pyleman, Cremers-Opdebeeck, Richard Depasse).

DECLARATION OF COMPETING INTEREST

D.G. is a cofounder of AaviGen GmbH. F.M. works at Spark Therapeutics. D.G., J.E.A., T.V., M.K.C. and W.T. are inventors on patent applications related to this work. All other authors declare that they have no competing interests. The AAV plasmid bearing the GAA expression cassette including a full map can be obtained via an MTA from the Vrije Universiteit Brussel. The AAVMYO3 helper plasmid including a full map can easily be obtained by academic institutions via a standard non-commercial MTA from Heidelberg University Hospital.

DATA AVAILABILITY

Data will be made available on request.

APPENDIX A. SUPPLEMENTARY DATA

Supplementary data to this article can be found online at https://doi.org/10.1016/j.molmet.2024.101899.

REFERENCES

[1] van der Ploeg AT, Reuser AJ. Pompe's disease. Lancet 2008. https://doi.org/10.1016/S0140-6736(08)61555-X.

[2] Sidman RL, Taksir T, Fidler J, Zhao M, Dodge JC, Passini MA, et al. Temporal neuropathologic and behavioral phenotype of 6 neo/6 neo Pompe pisease mice. J Neuropathol Exp Neurol 2008;67(8). https://doi.org/10.1097/NEN.0b013e3181815994.

[3] DeRuisseau LR, Fuller DD, Qiu K, DeRuisseau KC, Donnelly WH, Mah C, et al. Neural deficits contribute to respiratory insufficiency in Pompe disease. Proc Natl Acad Sci USA 2009;106(23):9419—24. https://doi.org/10.1073/pnas.0902534106.

[4] Korlimarla A, Lim J-A, Kishnani PS, Sun B. An emerging phenotype of central nervous system involvement in Pompe disease: from bench to bedside and beyond. Ann Transl Med 2019;7(13):289. https://doi.org/10.21037/atm.2019.04.49. 289.

[5] Stevens D, Milani-Nejad S, Mozaffar T. Pompe disease: a clinical, diagnostic, and therapeutic overview. Curr Treat Options Neurol 2022;24(11):573—88. https://doi.org/10.1007/s11940-022-00736-1.

[6] Ronzitti G, Collaud F, Laforet P, Mingozzi F. Progress and challenges of gene therapy for Pompe disease. Ann Transl Med 2019;7(13). https://doi.org/10.21037/atm.2019.04.67.

[7] Colella P, Mingozzi F. Gene therapy for pompe disease: the time is now. Hum Gene Ther 2019. https://doi.org/10.1089/hum.2019.109.

[8] Unnisa Z, Yoon JK, Schindler JW, Mason C, van Til NP. Gene therapy developments for pompe disease. Biomedicines 2022. https://doi.org/10.3390/biomedicines10020302.

[9] Fraites TJ, Schleissing MR, Shanely RA, Walter GA, Cloutier DA, Zolotukhin I, et al. Correction of the enzymatic and functional deficits in a model of pompe disease using adeno-associated virus vectors. Mol Ther 2002;5(5). https://doi.org/10.1006/mthe.2002.0580.

[10] Sun B, Zhang H, Franco LM, Brown T, Bird A, Schneider A, et al. Correction of glycogen storage disease type II by an adeno-associated virus vector containing a muscle-specific promoter. Mol Ther 2005;11(6). https://doi.org/10.1016/j.ymthe.2005.01.012.

[11] Mah CS, Falk DJ, Germain SA, Kelley JS, Lewis MA, Cloutier DA, et al. Gel-mediated delivery of AAV1 vectors corrects ventilatory function in pompe mice with established disease. Mol Ther 2010;18(3):502–10. https://doi.org/10.1038/mt.2009.305.

[12] Kohler L, Puertollano R, Raben N. Pompe disease: from basic science to therapy. Neurotherapeutics 2018;15(4):928–42. https://doi.org/10.1007/s13311-018-0655-y.

[13] Puzzo F, Colella P, Biferi MG, Bali D, Paulk NK, Vidal P, et al. Rescue of Pompe disease in mice by AAV-mediated liver delivery of secretable acid α-glucosidase. Sci Transl Med 2017;9(418). https://doi.org/10.1126/scitranslmed.aam6375.

[14] Colella P, Sellier P, Costa Verdera H, Puzzo F, van Wittenberghe L, Guerchet N, et al. AAV gene transfer with tandem promoter design prevents anti-transgene immunity and provides persistent efficacy in neonate pompe mice. Molecular Therapy - Methods and Clinical Development 2019;12. https://doi.org/10.1016/j.omtm.2018.11.002.

[15] Colella P, Sellier P, Gomez MJ, Biferi MG, Tanniou G, Guerchet N, et al. Gene therapy with secreted acid alpha-glucosidase rescues Pompe disease in a novel mouse model with early-onset spinal cord and respiratory defects. EBioMedicine 2020;61. https://doi.org/10.1016/j.ebiom.2020.103052.

[16] Cagin U, Puzzo F, Gomez MJ, Moya-Nilges M, Sellier P, Abad C, et al. Rescue of advanced pompe disease in mice with hepatic expression of secretable acid α-glucosidase. Mol Ther 2020;28(9). https://doi.org/10.1016/j.ymthe.2020.05.025.

[17] Costa-Verdera H, Collaud F, Riling CR, Sellier P, Nordin JML, Preston GM, et al. Hepatic expression of GAA results in enhanced enzyme bioavailability in mice and non-human primates. Nat Commun 2021;12(1). https://doi.org/10.1038/s41467-021-26744-4.

[18] Sun B, Zhang H, Franco LM, Young SP, Schneider A, Bird A, et al. Efficacy of an adeno-associated virus 8-pseudotyped vector in glycogen storage disease type II. Mol Ther 2005;11(1). https://doi.org/10.1016/j.ymthe.2004.10.004.

[19] Sun B, Young SP, Li P, Di C, Brown T, Salva MZ, et al. Correction of multiple striated muscles in murine pompe disease through adeno-associated virus-mediated gene therapy. Mol Ther 2008;16(8). https://doi.org/10.1038/mt.2008.133.

[20] Falk DJ, Soustek MS, Todd AG, Mah CS, Cloutier DA, Kelley JS, et al. Comparative impact of AAV and enzyme replacement therapy on respiratory and cardiac function in adult Pompe mice. Molecular Therapy - Methods and Clinical Development 2015;2. https://doi.org/10.1038/mtm.2015.7.

[21] Keeler AM, Zieger M, Todeasa SH, McCall AL, Gifford JC, Birsak S, et al. Systemic delivery of AAVB1-GAA clears glycogen and prolongs survival in a mouse model of pompe disease. Hum Gene Ther 2019;30(1). https://doi.org/10.1089/hum.2018.016.

[22] Lim J-A, Yi H, Gao F, Raben N, Kishnani PS, Sun B. Intravenous injection of an AAV-PHP.B vector encoding human acid α-glucosidase rescues both muscle and CNS defects in murine pompe disease. Molecular Therapy - Methods & Clinical Development 2019;12:233–45. https://doi.org/10.1016/j.omtm.2019.01.006.

[23] Eggers M, Vannoy CH, Huang J, Purushothaman P, Brassard J, Fonck C, et al. Muscle-directed gene therapy corrects Pompe disease and uncovers species-specific GAA immunogenicity. EMBO Mol Med 2022;14(1). https://doi.org/10.15252/emmm.202113968.

[24] Wang L, Wang H, Bell P, McMenamin D, Wilson JM. Hepatic gene transfer in neonatal mice by adeno-associated virus serotype 8 vector. Hum Gene Ther 2012;23(5):533–9. https://doi.org/10.1089/hum.2011.183.

[25] Bortolussi G, Zentillin L, Vaníkova J, Bockor L, Bellarosa C, Mancarella A, et al. Life-long correction of hyperbilirubinemia with a neonatal liver-specific AAV-mediated gene transfer in a lethal mouse model of Crigler-Najjar syndrome. Hum Gene Ther 2014;25(9). https://doi.org/10.1089/hum.2013.233.

[26] Piccolo P, Rossi A, Brunetti-Pierri N. Liver-directed gene-based therapies for inborn errors of metabolism. Expet Opin Biol Ther 2021. https://doi.org/10.1080/14712598.2020.1817375.

[27] Dowling JJ, Müller-Felber W, Smith BK, Bönnemann CG, Kuntz NL, Muntoni F, et al. INCEPTUS natural history, run-in study for gene replacement clinical trial in X-linked myotubular myopathy. J Neuromuscul Dis 2022;9(4):503–16. https://doi.org/10.3233/JND-210781.

[28] Tulalamba W, Weinmann J, Pham QH, El Andari J, VandenDriessche T, Chuah MK, et al. Distinct transduction of muscle tissue in mice after systemic delivery of AAVpo1 vectors. Gene Ther 2020;27(3–4). https://doi.org/10.1038/s41434-019-0106-3.

[29] Weinmann J, Weis S, Sippel J, Tulalamba W, Remes A, El Andari J, et al. Identification of a myotropic AAV by massively parallel in vivo evaluation of barcoded capsid variants. Nat Commun 2020;11(1). https://doi.org/10.1038/s41467-020-19230-w.

[30] Tabebordbar M, Lagerborg KA, Stanton A, King EM, Ye S, Tellez L, et al. Directed evolution of a family of AAV capsid variants enabling potent muscle-directed gene delivery across species. Cell 2021;184(19). https://doi.org/10.1016/j.cell.2021.08.028.

[31] El Andari J, Renaud-Gabardos E, Tulalamba W, Weinmann J, Mangin L, Pham QH, et al. Semirational bioengineering of AAV vectors with increased potency and specificity for systemic gene therapy of muscle disorders. Sci Adv 2022;8(38). https://doi.org/10.1126/sciadv.abn4704.

[32] Sarcar S, Tulalamba W, Rincon MY, Tipanee J, Pham HQ, Evens H, et al. Next-generation muscle-directed gene therapy by in silico vector design. Nat Commun 2019;10(1). https://doi.org/10.1038/s41467-018-08283-7.

[33] Raben N, Nagaraju K, Lee E, Kessler P, Byrne B, Lee L, et al. Targeted disruption of the acid α-glucosidase gene in mice causes an illness with critical features of both infantile and adult human glycogen storage disease type II. J Biol Chem 1998;273(30). https://doi.org/10.1074/jbc.273.30.19086.

[34] Bijvoet AG, van de Kamp EH, Kroos MA, Ding JH, Yang BZ, Visser P, et al. Generalized glycogen storage and cardiomegaly in a knockout mouse model of Pompe disease. Hum Mol Genet 1998;7(1):53–62. https://doi.org/10.1093/hmg/7.1.53.

[35] Bijvoet AGA, Van Hirtum H, Vermey M, Van Leenen D, Van der Ploeg AT, Mooi WJ, et al. Pathological features of glycogen storage disease type II highlighted in the knockout mouse model. J Pathol 1999;189(3):416–24. https://doi.org/10.1002/(SICI)1096-9896(199911)189:3<416::AID-PATH445>3.0.CO;2-424.

[36] Bijvoet AGA, Van Hirtum H, Kroos MA, Van de Kamp EHM, Schoneveld O, Visser P, et al. Human acid -glucosidase from rabbit milk has therapeutic effect in mice with glycogen storage disease type II. Hum Mol Genet 1999;8(12):2145–53. https://doi.org/10.1093/hmg/8.12.2145.

[37] Raben N, Nagaraju K, Lee E, Plotz P. Modulation of disease severity in mice with targeted disruption of the acid α-glucosidase gene. Neuromuscul Disord 2000;10(4–5):283–91. https://doi.org/10.1016/S0960-8966(99)00117-0.

[38] Byrne BJ, Collins S, Mah C, Smith B, Conlon T, Martin D, et al. Phase I/II trial of diaphragm delivery of recombinant adeno-associated virus acid alpha-glucosidase (rAAaV1-CMV-GAA) gene vector in patients with pompe disease. Human Gene Therapy Clinical Development 2014;25(3). https://doi.org/10.1089/humc.2014.2514.

[39] Huang JY, Kan SH, Sandfeld EK, Dalton ND, Rangel AD, Chan Y, et al. CRISPR-Cas9 generated Pompe knock-in murine model exhibits early-onset

hypertrophic cardiomyopathy and skeletal muscle weakness. Sci Rep 2020;10(1). https://doi.org/10.1038/s41598-020-65259-8.

[40] Kan S, Huang JY, Harb J, Rha A, Dalton ND, Christensen C, et al. CRISPR-mediated generation and characterization of a Gaa homozygous c.1935C>A (p.D645E) Pompe disease knock-in mouse model recapitulating human infantile onset-Pompe disease. Sci Rep 2022;12(1):21576. https://doi.org/10.1038/s41598-022-25914-8.

[41] Ayuso E, Mingozzi F, Montane J, Leon X, Anguela XM, Haurigot V, et al. High AAV vector purity results in serotype- and tissue-independent enhancement of transduction efficiency. Gene Ther 2010;17(4). https://doi.org/10.1038/gt.2009.157.

[42] Casana E, Jimenez V, Sacristan V, Muñoz S, Jambrina C, Rodó J, et al. BMP7 overexpression in adipose tissue induces white adipogenesis and improves insulin sensitivity in ob/ob mice. Int J Obes 2021;45(2). https://doi.org/10.1038/s41366-020-00700-6.

[43] Muñoz S, Franckhauser S, Elias I, Ferré T, Hidalgo A, Monteys AM, et al. Chronically increased glucose uptake by adipose tissue leads to lactate production and improved insulin sensitivity rather than obesity in the mouse. Diabetologia 2010;53(11). https://doi.org/10.1007/s00125-010-1840-7.

[44] Ruzo A, Garcia M, Ribera A, Villacampa P, Haurigot V, Marcó S, et al. Liver production of sulfamidase reverses peripheral and ameliorates CNS pathology in mucopolysaccharidosis IIIA mice. Mol Ther 2012;20(2). https://doi.org/10.1038/mt.2011.220.

[45] Iyer V, Shen B, Zhang W, Hodgkins A, Keane T, Huang X, et al. Off-target mutations are rare in Cas9-modified mice. Nat Methods 2015. https://doi.org/10.1038/nmeth.3408.

[46] Ayabe S, Nakashima K, Yoshiki A. Off- and on-target effects of genome editing in mouse embryos. J Reprod Dev 2019;65(1). https://doi.org/10.1262/jrd.2018-128.

[47] Kishnani PS, Hwu WL, Mandel H, Nicolino M, Yong F, Corzo D. A retrospective, multinational, multicenter study on the natural history of infantile-onset Pompe disease. J Pediatr 2006;148(5). https://doi.org/10.1016/j.jpeds.2005.11.033.

[48] Thurberg BL, Lynch Maloney C, Vaccaro C, Afonso K, Tsai AC-H, Bossen E, et al. Characterization of pre- and post-treatment pathology after enzyme replacement therapy for pompe disease. Lab Invest 2006;86(12):1208–20. https://doi.org/10.1038/labinvest.3700484.

[49] Schänzer A, Kaiser A-K, Mühlfeld C, Kulessa M, Paulus W, von Pein H, et al. Quantification of muscle pathology in infantile Pompe disease. Neuromuscul Disord 2017;27(2):141–52. https://doi.org/10.1016/j.nmd.2016.10.010.

[50] Winkel LPF, Kamphoven JHJ, Van Den Hout HJMP, Severijnen LA, Van Doorn PA, Reuser AJJ, et al. Morphological changes in muscle tissue of patients with infantile Pompe's disease receiving enzyme replacement therapy. Muscle Nerve 2003;27(6):743–51. https://doi.org/10.1002/mus.10381.

[51] Prater SN, Patel TT, Buckley AF, Mandel H, Vlodavski E, Banugaria SG, et al. Skeletal muscle pathology of infantile Pompe disease during long-term enzyme replacement therapy. Orphanet J Rare Dis 2013;8(1):90. https://doi.org/10.1186/1750-1172-8-90.

[52] Moriggi M, Capitanio D, Torretta E, Barbacini P, Bragato C, Sartori P, et al. Muscle proteomic profile before and after enzyme replacement therapy in late-onset pompe disease. Int J Mol Sci 2021;22(6):2850. https://doi.org/10.3390/ijms22062850.

[53] Di Rocco M, Buzzi D, Tarò M. Glycogen storage disease type II: clinical overview. Acta Myol 2007;26(1).

[54] Wu J, Dang Y, Su W, Liu C, Ma H, Shan Y, et al. Molecular cloning and characterization of rat LC3A and LC3B - two novel markers of autophagosome. Biochem Biophys Res Commun 2006;339(1). https://doi.org/10.1016/j.bbrc.2005.10.211.

[55] Glick D, Barth S, Macleod KF. Autophagy: cellular and molecular mechanisms. J Pathol 2010. https://doi.org/10.1002/path.2697.

[56] Liu WJ, Ye L, Huang WF, Guo LJ, Xu ZG, Wu HL, et al. p62 links the autophagy pathway and the ubiqutin-proteasome system upon ubiquitinated protein degradation. Cell Mol Biol Lett 2016. https://doi.org/10.1186/s11658-016-0031-z.

[57] Sardiello M, Palmieri M, Ronza A Di, Medina DL, Valenza M, Gennarino VA, et al. A gene network regulating lysosomal biogenesis and function. Science 2009;325(5939). https://doi.org/10.1126/science.1174447.

[58] Marcò S, Pujol A, Roca C, Motas S, Ribera A, Garcia M, et al. Progressive neurologic and somatic disease in a novel mouse model of human mucopolysaccharidosis type IIIC. DMM Disease Models and Mechanisms 2016;9(9). https://doi.org/10.1242/dmm.025171.

[59] Slonim AE, Bulone L, Ritz S, Goldberg T, Chen A, Martiniuk F. Identification of two subtypes of infantile acid maltase deficiency. J Pediatr 2000;137(2):283–5. https://doi.org/10.1067/mpd.2000.107112.

[60] van den Hout HMP, Hop W, van Diggelen OP, Smeitink JAM, Smit GPA, Poll-The B-TT, et al. The natural course of infantile pompe's disease: 20 original cases compared with 133 cases from the literature. Pediatrics 2003;112(2):332–40. https://doi.org/10.1542/peds.112.2.332.

[61] Marsden D. Infantile onset Pompe disease: a report of physician narratives from an epidemiologic study. Genet Med 2005;7(2):147–50. https://doi.org/10.1097/01.GIM.0000154301.76619.5C.

[62] Clarke J, Kayatekin C, Viel C, Shihabuddin L, Sardi SP. Murine models of lysosomal storage diseases exhibit differences in brain protein aggregation and neuroinflammation. Biomedicines 2021;9(5):446. https://doi.org/10.3390/biomedicines9050446.

[63] Gibbs RA, Weinstock GM, Metzker ML, Muzny DM, Sodergren EJ, Scherer S, et al. Genome sequence of the Brown Norway rat yields insights into mammalian evolution. Nature 2004;428(6982). https://doi.org/10.1038/nature02426.

[64] Iannaccone PM, Jacob HJ. Rats! Disease Models & Mechanisms 2009;2(5–6):206–10. https://doi.org/10.1242/dmm.002733.

[65] Tessitore A, Faella A, O'Malley T, Cotugno G, Doria M, Kunieda T, et al. Biochemical, pathological, and skeletal improvement of mucopolysaccharidosis VI after gene transfer to liver but not to muscle. Mol Ther 2008;16(1). https://doi.org/10.1038/sj.mt.6300325.

[66] Larcher T, Lafoux A, Tesson L, Remy SV, Thepenier V, François V, et al. Characterization of dystrophin deficient rats: a new model for duchenne muscular dystrophy. PLoS One 2014;9(10). https://doi.org/10.1371/journal.pone.0110371.

[67] Lambert LJ, Challa AK, Niu A, Zhou L, Tucholski J, Johnson MS, et al. Increased trabecular bone and improved biomechanics in an osteocalcin-null rat model created by CRISPR/Cas9 technology. DMM Disease Models and Mechanisms 2016;9(10). https://doi.org/10.1242/dmm.025247.

[68] Bertolin J, Sánchez V, Ribera A, Jaén ML, Garcia M, Pujol A, et al. Treatment of skeletal and non-skeletal alterations of Mucopolysaccharidosis type IVA by AAV-mediated gene therapy. Nat Commun 2021;12(1). https://doi.org/10.1038/s41467-021-25697-y.

[69] Nakamura K, Tanaka T, Yamanouchi K. In vivo modeling of skeletal muscle diseases using the CRISPR/Cas9 system in rats. Methods Mol Biol 2023;2640:277–85. https://doi.org/10.1007/978-1-0716-3036-5_20.

[70] Dayton RD, Grames MS, Klein RL. More expansive gene transfer to the rat CNS: AAV PHP.EB vector dose–response and comparison to AAV PHP.B. Gene Therapy 2018;25(5):392–400. https://doi.org/10.1038/s41434-018-0028-5.

[71] Jackson KL, Dayton RD, Klein RL. AAV9 supports wide-scale transduction of the CNS and TDP-43 disease modeling in adult rats. Molecular Therapy - Methods Clinical Develop 2015;2:15036. https://doi.org/10.1038/mtm.2015.36.

[72] Buchlis G, Podsakoff GM, Radu A, Hawk SM, Flake AW, Mingozzi F, et al. Factor IX expression in skeletal muscle of a severe hemophilia B patient 10

years after AAV-mediated gene transfer. Blood 2012;119(13). https://doi.org/10.1182/blood-2011-09-382317.

[73] Gaudet D, Méthot J, Déry S, Brisson D, Essiembre C, Tremblay G, et al. Efficacy and long-term safety of alipogene tiparvovec (AAV1-LPL S447X) gene therapy for lipoprotein lipase deficiency: an open-label trial. Gene Ther 2013;20(4). https://doi.org/10.1038/gt.2012.43.

[74] Nathwani AC, Reiss UM, Tuddenham EGD, Rosales C, Chowdary P, McIntosh J, et al. Long-term safety and efficacy of factor IX gene therapy in hemophilia B. N Engl J Med 2014;371(21). https://doi.org/10.1056/nejmoa1407309.

[75] Bennett J, Wellman J, Marshall KA, McCague S, Ashtari M, DiStefano-Pappas J, et al. Safety and durability of effect of contralateral-eye administration of AAV2 gene therapy in patients with childhood-onset blindness caused by RPE65 mutations: a follow-on phase 1 trial. Lancet 2016;388(10045). https://doi.org/10.1016/S0140-6736(16)30371-3.

[76] Mendell JR, Al-Zaidy S, Shell R, Arnold WD, Rodino-Klapac LR, Prior TW, et al. Single-dose gene-replacement therapy for spinal muscular atrophy. N Engl J Med 2017;377(18). https://doi.org/10.1056/nejmoa1706198.

[77] Marcó S, Haurigot V, Bosch F. In vivo gene therapy for mucopolysaccharidosis type III (sanfilippo syndrome): a new treatment Horizon. Hum Gene Ther 2019. https://doi.org/10.1089/hum.2019.217.

[78] Corti M, Liberati C, Smith BK, Lawson LA, Tuna IS, Conlon TJ, et al. Safety of intradiaphragmatic delivery of adeno-associated virus-mediated alpha-glucosidase (rAAV1-CMV-hGAA) gene therapy in children affected by pompe disease. Human Gene Therapy Clinical Develop 2017;28(4). https://doi.org/10.1089/humc.2017.146.

[79] Nakai H, Yant SR, Storm TA, Fuess S, Meuse L, Kay MA. Extrachromosomal recombinant adeno-associated virus vector genomes are primarily responsible for stable liver transduction in vivo. J Virol 2001;75(15). https://doi.org/10.1128/jvi.75.15.6969-6976.2001.

[80] Wang L, Bell P, Lin J, Calcedo R, Tarantal AF, Wilson JM. AAV8-mediated hepatic gene transfer in infant rhesus monkeys (macaca mulatta). Mol Ther 2011;19(11). https://doi.org/10.1038/mt.2011.151.

[81] Wang L, Wang H, Bell P, McMenamin D, Wilson JM. Hepatic gene transfer in Neonatal mice by Adeno-associated virus serotype 8 vector. Hum Gene Ther 2012;23(5). https://doi.org/10.1089/hum.2011.183.

[82] Corti M, Cleaver B, Clément N, Conlon TJ, Faris KJ, Wang G, et al. Evaluation of readministration of a recombinant adeno-associated virus vector expressing acid alpha-glucosidase in pompe disease: preclinical to clinical planning. Human Gene Therapy Clinical Develop 2015;26(3). https://doi.org/10.1089/humc.2015.068.

[83] Meliani A, Boisgerault F, Hardet R, Marmier S, Collaud F, Ronzitti G, et al. Antigen-selective modulation of AAV immunogenicity with tolerogenic rapamycin nanoparticles enables successful vector re-administration. Nat Commun 2018;9(1). https://doi.org/10.1038/s41467-018-06621-3.

[84] Leborgne C, Barbon E, Alexander JM, Hanby H, Delignat S, Cohen DM, et al. IgG-cleaving endopeptidase enables in vivo gene therapy in the presence of anti-AAV neutralizing antibodies. Nat Med 2020;26(7). https://doi.org/10.1038/s41591-020-0911-7.

[85] George LA, Ragni MV, Rasko JEJ, Raffini LJ, Samelson-Jones BJ, Ozelo M, et al. Long-term follow-up of the first in human intravascular delivery of AAV for gene transfer: AAV2-hFIX16 for severe hemophilia B. Mol Ther 2020;28(9). https://doi.org/10.1016/j.ymthe.2020.06.001.

[86] Rucker M, Fraites TJ, Porvasnik SL, Lewis MA, Zolotukhin I, Cloutier DA, et al. Rescue of enzyme deficiency in embryonic diaphragm in a mouse model of metabolic myopathy: pompe disease. Development 2004;131(12):3007–19. https://doi.org/10.1242/dev.01169.

[87] Mah C, Cresawn KO, Fraites TJ, Pacak CA, Lewis MA, Zolotukhin I, et al. Sustained correction of glycogen storage disease type II using adeno-associated virus serotype 1 vectors. Gene Ther 2005;12(18):1405–9. https://doi.org/10.1038/sj.gt.3302550.

[88] Mah C, Pacak CA, Cresawn KO, DeRuisseau LR, Germain S, Lewis MA, et al. Physiological correction of pompe disease by systemic delivery of adeno-associated virus serotype 1 vectors. Mol Ther 2007;15(3):501–7. https://doi.org/10.1038/sj.mt.6300100.

[89] Conlon TJ, Mah CS, Pacak CA, Rucker Henninger MB, Erger KE, Jorgensen ML, et al. Transfer of therapeutic genes into fetal rhesus monkeys using recombinant adeno-associated type i viral vectors. Human Gene Therapy Clinical Develop 2016;27(4). https://doi.org/10.1089/humc.2016.119.

[90] Mendell JR, Sahenk Z, Lehman K, Nease C, Lowes LP, Miller NF, et al. Assessment of systemic delivery of rAAVrh74.MHCK7.micro-dystrophin in children with duchenne muscular dystrophy: a nonrandomized controlled trial. JAMA Neurol 2020;77(9). https://doi.org/10.1001/jamaneurol.2020.1484.

[91] Sun B, Zhang H, Bird A, Li S, Young SP, Koeberl DD. Impaired clearance of accumulated lysosomal glycogen in advanced Pompe disease despite high-level vector-mediated transgene expression. J Gene Med 2009;11(10):913–20. https://doi.org/10.1002/jgm.1372.

[92] Vandendriessche T, Thorrez L, Acosta-Sanchez A, Petrus I, Wang L, Ma L, et al. Efficacy and safety of adeno-associated viral vectors based on serotype 8 and 9 vs. lentiviral vectors for hemophilia B gene therapy. J Thromb Haemostasis 2007;5(1):16–24. https://doi.org/10.1111/j.1538-7836.2006.02220.x.

[93] Sawada T, Kido J, Nakamura K. Newborn screening for pompe disease. Int J Neonatal Screening 2020;6(2):31. https://doi.org/10.3390/ijns6020031.

[94] Schaaf GJ, van Gestel TJ, Brusse E, Verdijk RM, de Coo IF, van Doorn PA, et al. Lack of robust satellite cell activation and muscle regeneration during the progression of Pompe disease. Acta Neuropathologica Commun 2015;3(1):65. https://doi.org/10.1186/s40478-015-0243-x.

[95] Schaaf GJ, van Gestel TJM, in't Groen SLM, de Jong B, Boomaars B, Tarallo A, et al. Satellite cells maintain regenerative capacity but fail to repair disease-associated muscle damage in mice with Pompe disease. Acta Neuropathologica Commun 2018;6(1):119. https://doi.org/10.1186/s40478-018-0620-3.

[96] Lagalice L, Pichon J, Gougeon E, Soussi S, Deniaud J, Ledevin M, et al. Satellite cells fail to contribute to muscle repair but are functional in Pompe disease (glycogenosis type II). Acta Neuropathologica Commun 2018;6(1):116. https://doi.org/10.1186/s40478-018-0609-y.

[97] Schaaf GJ, Canibano-Fraile R, van Gestel TJM, van der Ploeg AT, Pijnappel WWMP. Restoring the regenerative balance in neuromuscular disorders: satellite cell activation as therapeutic target in Pompe disease. Ann Transl Med 2019;7(13):280. https://doi.org/10.21037/atm.2019.04.48.

[98] Ganassi M, Zammit PS. Involvement of muscle satellite cell dysfunction in neuromuscular disorders: expanding the portfolio of satellite cell-opathies. Eur J Transl Myology 2022;32(1). https://doi.org/10.4081/ejtm.2022.10064.

[99] Chand DH, Zaidman C, Arya K, Millner R, Farrar MA, Mackie FE, et al. Thrombotic microangiopathy following onasemnogene abeparvovec for spinal muscular atrophy: a case series. J Pediatr 2021;231. https://doi.org/10.1016/j.jpeds.2020.11.054.

[100] Mendell JR, Al-Zaidy SA, Rodino-Klapac LR, Goodspeed K, Gray SJ, Kay CN, et al. Current clinical applications of in vivo gene therapy with AAVs. Mol Ther 2021. https://doi.org/10.1016/j.ymthe.2020.12.007.

[101] Mullard A. Gene therapy community grapples with toxicity issues, as pipeline matures. Nat Rev Drug Discov 2021. https://doi.org/10.1038/d41573-021-00164-x.

[102] Sabatino DE, Bushman FD, Chandler RJ, Crystal RG, Davidson BL, Dolmetsch R, et al. Evaluating the state of the science for adeno-associated virus integration: an integrated perspective. Mol Ther 2022;30(8):2646–63. https://doi.org/10.1016/j.ymthe.2022.06.004.

[103] Hinderer C, Katz N, Buza EL, Dyer C, Goode T, Bell P, et al. Severe toxicity in nonhuman primates and piglets following high-dose intravenous administration of an adeno-associated virus vector expressing human SMN. Hum Gene Ther 2018;29(3):285–98. https://doi.org/10.1089/hum.2018.015.

[104] Hordeaux J, Buza EL, Dyer C, Goode T, Mitchell TW, Richman L, et al. Adeno-associated virus-induced dorsal root ganglion pathology. Hum Gene Ther 2020;31(15–16). https://doi.org/10.1089/hum.2020.167.

